The integration mechanism of the four positional cues —anterior, posterior, dorsal, and ventral—in axolotl limb regeneration

Sakiya Yamamoto[1], Saya Furukawa[1], Ayaka Ohashi[1], Mayuko Hamada [1, 2], and Akira Satoh[1]

Affiliations:

[1] Okayama University, Graduate School of Environmental, Life, Natural Science and Technology, Okayama, Japan

[2] Ushimado Marine Institute (UMI), Okayama University, Okayama, Japan

*Corresponding author

Akira Satoh, Ph.D.,

Okayama University, Okayama University, Graduate School of Environmental, Life, Natural Science and Technology

Email: satoha@cc.okayama-u.ac.jp

Tel: +81-86-251-8421

Abstract

Axolotls (*Ambystoma mexicanum*) exhibit a remarkable ability to regenerate limbs after amputation. Classical experiments have suggested that the integration of four positional cues—dorsal, ventral, anterior, and posterior—within a regenerating blastema is necessary for accurate limb pattern formation. However, the molecular basis underlying this integration has remained largely unknown. Here, we demonstrate that both dorsal and ventral tissues are required for limb formation via induction of *Shh* expression, which plays a crucial role in limb patterning. Using the accessory limb model (ALM), we induced position-specific blastemas lacking cells derived from a single orientation (anterior, posterior, dorsal, or ventral). Patterned limb formation occurred only in blastemas containing both dorsal- and ventral-derived cells. We further observed that *Shh* expression requires dorsoventral contact within a blastema, highlighting the necessity of dorsoventral contact for inducing *Shh* expression. Additionally, we identified molecules mediating dorsoventral-dependent *Shh* expression: WNT10B as the dorsal factor and FGF2 as the ventral factor. Our findings clarify the role of dorsal and ventral positional cues in inducing *Shh*, a mechanism that has rarely been studied in the context of limb regeneration and pattern formation. This model provides new insights into how interpositional interactions are integrated to drive the regeneration process.

Introduction

Axolotls (*Ambystoma mexicanum*) possess remarkable regenerative abilities, enabling the regeneration of entire limbs after amputation. Among tetrapods (four-limbed vertebrates), only urodele amphibians retain the lifelong ability to regenerate fully developed limbs. Investigating the molecular mechanisms underlying axolotl limb regeneration could provide valuable insights for advancing regenerative medicine in humans, potentially leading to new therapies for tissue repair and organ regeneration.

The limb regeneration process can be divided into two stages: the blastema (regenerating limb primordium) induction process and the limb patterning process. The induction of a blastema, which contains highly proliferative multipotent and unipotent cells, depends on the presence of nerves at the injured region. When a denervated limb is amputated, a blastema is not induced (Todd, 1823). The blastema induction process is followed by the limb patterning process. In limb development, positional values are thought to be established along three-dimensional axes—anteroposterior, dorsoventral, and proximodistal—based on positional information. For example, WNT7A, secreted from dorsal ectoderm, acts as dorsal positional information to induce *Lmx1b* expression, which acts as dorsal positional value, in underlying mesenchymal cells (Riddle et al., 1995; Vogel et al., 1995; Cygan et al., 1997; Chen et al., 1998; Chen, 2002). Similarly, SHH is known to serve as posterior positional information, regulating anteroposterior patterning (Riddle et al., 1993). For successful limb patterning in limb regeneration, interactions among anterior, posterior, dorsal, and ventral cells within a blastema have been considered essential. The importance of these interpositional interactions was investigated in creating double-half limbs. Amputating the double-half limbs can provide a blastema in a “one-positional-value-missing” state. For example, when a double-dorsal limb is amputated, the resulting blastema lacks ventral positional value. Such blastemas form hypomorphic, spike-like structures or fail to regenerate entirely (Bryant, 1976; Bryant and Baca, 1978; Burton et al., 1986). It is noteworthy that structural patterns along the anteroposterior axis have been lost, even though both anterior and posterior cells should be present in a blastema induced from double-dorsal and double-ventral limb. Additional experiments involving ectopic contact between opposite regions (e.g., anterior-posterior or dorsal-ventral) of a blastema further support the critical role of interpositional interactions in the limb patterning process, as such interactions can lead to ectopic limb formation (Iten and Bryant, 1975; Bryant and Iten, 1976; Maden, 1980; Stocum, 1982). These findings suggest that specific signals from all four positional domains must be integrated for successful limb patterning, such that the absence of any one of them leads to failure. In the present study, we define these position-specific signals required for a blastema to form a limb as “positional cues.” We distinguish “positional cues” from “positional information” to clarify their distinct roles: positional information refers to signals that induce positional values within recipient cells, whereas positional cues do not necessarily induce positional values and may

act downstream of positional values. For example, WNT7A from the dorsal ectoderm in amniote limb development functions as dorsal positional information because it induces the dorsal positional values within the underlying mesenchyme. In contrast, FGF8 from the anterior region in axolotl limb regeneration functions as the anterior positional cue because it can substitute for anterior tissues in the limb patterning process (Nacu et al., 2016). Of course, these definitions are not mutually exclusive. One important feature of positional cue molecules is that they can substitute for tissues of one orientation in limb regeneration. To further understand limb regeneration, the molecular basis of the integration of the positional cues in limb patterning process should be elucidated.

The accessory limb model (ALM), a non-amputation experimental system, provides a valuable approach for studying axolotl limb regeneration, particularly the role of interpositional interactions (Endo et al., 2015). In this model, a blastema is induced through skin wounding combined with nerve deviation (Endo et al., 2004, Satoh et al., 2007). When ALM surgery is performed on the anterior side, the induced blastema (ALM blastema) lacks posterior-derived cells and is unable to form a properly patterned limb. This limitation can be overcome by supplying posterior-derived cells via a skin graft from the posterior side, enabling the successful regeneration of a patterned limb. Similarly, an ALM blastema can be induced in a position-specific manner along the limb axes. In this case, the induced ALM blastema will lack cells from the opposite side. This condition allows the investigation of blastema induction and limb patterning by selectively removing cells from specific orientations of the limb. Analyzing the characteristics and developmental limitations of these ALM blastemas provides valuable insights into the positional cues that regulate axolotl limb regeneration.

The molecular basis of the interpositional interactions within a blastema in the limb patterning process has been partially elucidated (Nacu et al., 2016). In a normal blastema, *Fgf8* and *Shh* are expressed at the anterior and the posterior regions, respectively. A previous study demonstrated that FGF8 and SHH proteins can substitute for anterior and posterior tissues, respectively, to form a patterned limb. Moreover, these proteins function as mutually inductive signals, maintaining each other's expression. These findings suggest that FGF8 and SHH serve as the anterior and posterior positional cues, respectively. In contrast, the molecular basis of dorsal and ventral positional cues remains poorly understood. Previous studies have shown that retinoic acid supplementation can convert the dorsal positional value to the ventral, enabling patterned limb formation even in the absence of ventral tissues (Vieira et al., 2019). However, the ventral positional cue remains uncertain, as retinoic acid induces ventral positional values rather than acting as the ventral positional cue itself, suggesting the existence of another, downstream ventral positional cue. Consequently, the mechanisms underlying dorsal and ventral positional cues, as well as their

integration with anterior and posterior cues, remain unclear.

In the present study, we investigated the roles of dorsal and ventral positional cues in limb patterning. We confirmed the necessity of dorsoventral tissue contact for limb patterning using the ALM. We found that the induction of *Shh* expression was dependent on the co-existence of dorsal and ventral cells in axolotl limb regeneration. Furthermore, we identified *Wnt10b* and *Fgf2* as dorsal and ventral positional cues, respectively, by RNA-seq analysis, and confirmed that these genes mediate *Shh* expression in axolotl blastemas. Our results suggest that the crucial role of the dorsal and ventral positional cues in the limb patterning process is to induce *Shh* expression, thereby enabling anteroposterior interaction. This model provides a framework for understanding the integration of the four positional cues during axolotl limb regeneration.

Results

Dorsal-ventral tissue contact is required for limb regeneration in the ALM

We performed the ALM experiment on *Ambystoma mexicanum* to investigate whether dorsoventral tissue contact, as well as anteroposterior tissue contact, is required for limb regeneration (Fig. 1). The skin was removed from one side (anterior, posterior, dorsal, or ventral) of a limb, and the large nerve fibers running along the center of a limb (*Nervus medianus* and *N. ulnaris*, Fig. 1A) were dissected and rerouted to the wounded region. As mentioned before, we supplied the cells from the contralateral side of a limb as a skin graft in experimental conditions to ensure the presence of sufficient cells for patterned limb formation. We conducted eight types of ALM blastema inductions, which can be categorized into two groups: basic ALM blastemas and skin-grafted ALM blastemas. The basic ALM blastemas included anteriorly induced ALM blastema (AntBL), posteriorly induced ALM blastema (PostBL), dorsally induced ALM blastema (DorBL), and ventrally induced ALM blastema (VentBL), all of which should lack cells from the contralateral side. The skin-grafted ALM blastemas included AntBL with posterior skin grafting (AntBL+P), PostBL with anterior skin grafting (PostBL+A), DorBL with ventral skin grafting (DorBL+V), and VentBL with dorsal skin grafting (VentBL+D); these ALM blastemas should contain cells with all anteroposterior and dorsoventral orientations. For the ALM experiment, we defined the two large blood vessels running on the anterior and posterior sides at the stylopod level (*Vena cephalica* and *V. basilica*, Fig. 1A) as the anterior and posterior dorsoventral borders, respectively. At 10 days post-surgery (dps), an ALM blastema was observed in all experimental groups (Fig. 1B–I). Consistent with previous studies (Endo et al., 2004; Nacu et al., 2016), limbs with multiple digits were formed from AntBL+P and PostBL+A (Table 1, Fig. 1F, G), whereas AntBL and PostBL either regressed or formed bump structures (Table 1, Fig. 1B, C). Similarly, DorBL+V and VentBL+D formed limbs (Table 1, Fig. 1H, I), whereas most DorBL and VentBL either regressed or formed bump structures (Table 1, Fig. 1D, E). Notably, only 1 out of 12 DorBL formed a limb, which may have resulted from ventral tissue contamination, as the rerouted nerves originally ran along the ventral side of the humerus. In contrast, none of 22 VentBL formed multi-digit limbs. These results suggest that both dorsal and ventral tissues, as well as anterior and posterior tissues, are required for successful limb formation.

Gene expression patterns in ALM blastemas

To elucidate the characteristics of the ALM blastemas that typically fail to form limbs (AntBL, PostBL, DorBL, and VentBL), we analyzed gene expression patterns at 10 dps (Fig. 2). *Lmx1b*, a gene necessary and sufficient for establishing the dorsal identity in mesenchymal cells in developing limb buds (Vogel et al., 1995; Chen et al., 1998; Chen, 2002), was used as a dorsal marker because we previously reported that *Lmx1b* is exclusively expressed in dorsal-derived cells and can be activated in the ALM experiment (Iwata et al., 2020; Yamamoto et al., 2022). The expression

159 patterns of *Fgf8*, *Shh*, and *Lmx1b* were investigated using *in situ* hybridization (ISH). In AntBL and
160 PostBL, *Lmx1b* expression was restricted to the dorsal half of the blastemas (Fig. 2B, G; n=5/5 for
161 both), suggesting the presence of both dorsal and ventral tissues. These expression patterns
162 correspond to the anatomically defined dorsoventral borders (Fig. 1A). In contrast, *Lmx1b* was
163 expressed throughout the entire region of DorBL (Fig. 2L, n=6/6), whereas no *Lmx1b* expression
164 was detected in VentBL (Fig. 2Q, n=6/6), suggesting the absence of ventral tissue in DorBL and
165 dorsal tissue in VentBL. Consistent with previous studies, *Fgf8* expression was observed in AntBL
166 (Fig. 2C, n=4/5), but not in PostBL (Fig. 2H, n=5/5, Nacu et al., 2016). Conversely, *Shh* expression
167 was detected in PostBL (Fig. 2I, n=5/5), but not in AntBL (Fig. 2D, n=5/5). In DorBL and VentBL,
168 *Shh* expression was largely absent (Fig. 2N, n = 5/6; Fig. 2S, n = 6/6), whereas *Fgf8* expression was
169 present in both (Fig. 2M, n = 4/6; Fig. 2R, n = 4/6). In DorBL, *Shh* expression was observed in only
170 1 out of 6 samples, possibly due to ventral tissue contamination, as described above. These results
171 suggest that *Fgf8* expression is independent of the co-existence of dorsal and ventral tissues, whereas
172 *Shh* expression appears to require their presence.
173
174 ***Induction of Shh expression requires both dorsal and ventral cells***
175 The absence of *Shh* expression in most DorBL and VentBL, combined with its consistent expression
176 in all PostBL—which contain both *Lmx1b*-positive and *Lmx1b*-negative regions—suggests that the
177 induction of *Shh* expression depends on the presence of both dorsal and ventral cells (Fig. 2). To test
178 this hypothesis, we performed cell-tracing experiments using GFP-expressing skin from transgenic
179 animals (Fig. 3). We induced VentBL in wild-type animals and then grafted the posterior half of the
180 dorsal skin (VentBL＋PD_{gfp}) or posterior half of the ventral skin (VentBL+PV_{gfp}) from GFP
181 transgenic animals (Fig. 3A). Similarly, DorBL was induced in wild-type animals, and the posterior
182 half of the dorsal skin (DorBL+PD_{gfp}) or the posterior half of the ventral skin (DorBL+PV_{gfp}) from
183 GFP transgenic animals was grafted (Fig. 3A). GFP-positive mesenchymal cells derived from the
184 posterior skin were expected to express *Shh* if provided with a suitable environment, because
185 posteriorly derived cells are known to have the competency to express *Shh* in a blastema (Iwata et
186 al., 2020). If the induction of *Shh* expression depends on the co-existence of dorsal and ventral cells,
187 *Shh* expression in the GFP-positive cells should be observed in VentBL+PD_{gfp} and DorBL+PV_{gfp} but
188 not in DorBL+PD_{gfp} or VentBL+PV_{gfp}. Samples were collected at 10 dps, and the expression of *Shh*
189 and *Lmx1b* was analyzed using ISH. In all four experimental groups, *Lmx1b* expression patterns in
190 the GFP-negative regions were consistent with those in DorBL and VentBL (Fig. 3D, F, H, J). In
191 DorBL+PD_{gfp} and VentBL+PD_{gfp}, *Lmx1b* expression was observed in GFP-positive mesenchymal
192 cells, whereas GFP-positive cells in DorBL+PV_{gfp} and VentBL+PV_{gfp} were *Lmx1b*-negative (Fig.

193 3C–F). These *Lmx1b* expression patterns suggest that dorsoventral tissue contact was present in
194 VentBL+PD$_{gfp}$ and DorBL+pV$_{gfp}$ but absent in DorBL+PD$_{gfp}$ and VentBL+PV$_{gfp}$. In the GFP-positive
195 cells derived from PD$_{gfp}$ skin, *Shh* expression was observed in VentBL+PD$_{gfp}$ (Fig. 3C, n=3/3) but
196 not in DorBL+PD$_{gfp}$ (Fig. 3E, n=3/3). Similarly, in the GFP-positive cells derived from PV$_{gfp}$ skin,
197 *Shh* expression was observed in DorBL+PV$_{gfp}$ (Fig3I, n=3/6) but not in VentBL+PV$_{gfp}$ (Fig. 3G,
198 n=7/7). In addition, *Shh* expression was observed in some GFP-negative mesenchymal cells in
199 samples where *Shh* expression was observed in GFP-positive cells. These results suggest that the
200 induction of *Shh* expression in posteriorly derived cells requires the co-existence of dorsal and
201 ventral cells.
202
203 ***Limb formation in the absence of dorsoventral tissue contact***
204 DorBL and VentBL failed to form limbs (Fig. 1D, E). *Shh* expression was absent in these blastemas,
205 whereas *Fgf8* was expressed (Fig. 2). Results from the cell-tracing experiments suggest that *Shh*
206 expression requires the co-existence of dorsal and ventral cells (Fig. 3). Based on these findings, we
207 hypothesized that while the co-existence of dorsal and ventral cells is necessary to induce *Shh*
208 expression, it is not directly required for limb patterning if SHH proteins are externally provided. To
209 test this hypothesis, we overexpressed *Shh* in DorBL and VentBL (Fig. 4A, B). As a positive control,
210 *Shh* was overexpressed in AntBL, where *Fgf8* was expressed but *Shh* expression was absent (Fig.
211 2C, D), as a previous study has shown that SHH supplementation to AntBL can induce limb
212 patterning (Nacu et al., 2016). As a result, *Shh*-electroporated AntBL, DorBL, and VentBL formed
213 limbs (n=10/19, 6/18, and 8/14, respectively, Fig. 4C–G). In contrast, GFP-electroporated DorBL
214 and VentBL (negative controls) failed to form limbs (n=7/7 and 6/6, respectively). We further
215 analyzed the anatomy of the induced limbs (Fig. 4H–K). We found that limbs formed from DorBL
216 and VentBL exhibited symmetric structures along the dorsoventral axis, suggesting double-dorsal
217 and double-ventral structures, respectively (Fig. 4J, K). In contrast, limbs formed from AntBL,
218 which contained both *Lmx1b*-positive and *Lmx1b*-negative regions (Fig. 2B), exhibited asymmetric
219 structures similar to those of normal limbs (Fig. 4H, I). To evaluate the symmetry of the limbs, we
220 applied a machine learning-based method using ilastic. Each pixel in the images was classified into
221 five classes (Classes 1 to 5, Fig. 4L). In this process, we annotated regions of background (Class 1),
222 cartilage (Class 2), muscle (Class 3), other connective tissue (Class 4), and epidermis (Class 5) as
223 training data for classification. Using these annotated regions as references, pixels were
224 automatically classified into the five classes. Each class was assumed to primarily represent these
225 tissues and regions with similar characteristics. Symmetry scores were then calculated for each class
226 individually and for the combined set of all classes (Fig. 4M–R, see Materials and Methods). The

227 analysis revealed that symmetry scores for Classes 2 and 3, which encompass cartilage and muscle,
228 and scores for the combined set of all classes were significantly higher in limbs formed from DorBL
229 and VentBL compared to intact limbs (Fig. 4N, O, R). In contrast, the differences in symmetry scores
230 for Classes 1, 4, and 5 in these limbs were relatively small (Fig. 4M, P, Q), likely because the axis of
231 symmetry was manually set to maximize the external shape as symmetrically as possible. No
232 significant differences in symmetry scores across all classes were observed between intact limbs and
233 limbs formed from AntBL. These results suggest that limbs formed from DorBL and VentBL exhibit
234 symmetric internal structures compared to normal limbs. Therefore, SHH supplementation appears
235 to compensate for the lack of co-existence of dorsal and ventral cells in limb patterning, without
236 inducing new dorsal or ventral identities. Thus, we conclude that the co-existence of both dorsal and
237 ventral cells is critical for inducing *Shh* expression, which in turn is essential for limb patterning.
238
239 ***The molecular basis of the dorsal and ventral positional cues***
240 To investigate the molecular basis of dorsal and ventral positional cues, we performed RNA-seq
241 analysis on DorBL and VentBL and identified differentially expressed genes (DEGs) between the
242 two groups ($p<0.05$, Fig. 5A). Among the DEGs, we specifically focused on genes annotated as
243 "intercellular signaling molecules" in PANTHER and identified 21 genes (Fig 5B). In this analysis,
244 we found that 5 genes were expressed at higher levels in DorBL and 16 genes were expressed at
245 higher levels in VentBL (Fig. 5B). Notably, *Wnt4*, *Wnt10b*, *Fgf2*, *Fgf7*, and *Tgfb2*, which encode
246 secreted proteins, belong to the WNT, FGF, and TGFB families, which play key roles in major
247 signaling pathways regulating limb developmental processes. To examine whether these genes
248 regulate the induction of *Shh* expression in ALM blastemas, we overexpressed each gene in either
249 DorBL or VentBL. As a result, *Shh* expression was observed in *Wnt10b*-electroporated VentBL
250 (n=3/3) and *Fgf2*-electroporated DorBL (n=5/7, Fig. 5C). In contrast, *Shh* expression was not
251 detected in *Wnt10b*-electroporated DorBL (n=4/4) or *Fgf2*-electroporated VentBL (n=3/3). Similarly,
252 *Shh* expression was not detected in *Fgf7*- or *Tgfb2*-electroporated DorBL (n=3/3 for both) or in
253 *Wnt4*-electroporated VentBL (n=4/4). To confirm *Shh* induction by FGF2 in DorBL, we supplied
254 commercially obtained mouse FGF2 proteins into DorBL via bead grafting and observed higher *Shh*
255 expression in DorBL with FGF2-soaked bead compared to DorBL with control DDW-soaked bead
256 (Fig. 5D). Next, to confirm *Shh* induction by WNT signaling in VentBL, we treated VentBL with 1
257 μM 6-bromoindirubin-3-oxime (GSK-3 Inhibitor, BIO). As a result, *Shh* expression was relatively
258 higher in BIO-treated VentBL compared to DMSO-treated control VentBL (Fig. 5E). Additionally,
259 symmetric limbs were formed in *Wnt10b*-electroporated VentBL (n=3/12), BIO-treated VentBL
260 (n=3/8), and in *Fgf2*-electroporated DorBL (n=5/10), being consistent with the results of *Shh*

overexpression (Fig. 5F–H, Fig. S1). These findings suggest that WNT10B, expressed highly in dorsal blastema cells, and FGF2, expressed highly in ventral blastema cells, function as the dorsal and ventral positional cues, respectively, to induce *Shh* expression, which subsequently supports limb patterning.

Limb formation without nerve deviation and ventral skin grafting

A previous study demonstrated that a cocktail of BMP2, FGF2, and FGF8 can substitute for nerve deviation in the ALM experiment on the anterior region, suggesting that nerves contribute to blastema induction by supplying these proteins (Makanae et al., 2014). We found that FGF2 can also substitute for ventral tissue in DorBL (Fig. 5), suggesting that FGF2 serves not only as part of the nerve factors in blastema induction but also as the ventral positional cue in limb patterning. To investigate whether supplementation with BMP2, FGF2, and FGF8 to the dorsal region could substitute for both nerve deviation and ventral skin grafting, we performed experiments involving gelatin beads soaked in these proteins (Fig. 6). The dorsal or ventral skin was removed at the zeugopod level, and a BMP2+FGF2+FGF8-soaked gelatin bead was grafted at 3 dps without nerve deviation. Blastema induction was observed in both experimental groups (Fig. 6A, B, upper panels). We investigated gene expression patterns in the induced blastemas and found that both *Fgf8* and *Shh* were expressed in blastemas induced at the dorsal site (n=8/8), whereas *Shh* expression was absent in ventral blastemas (n=5/5), although *Fgf8* expression was detected in most cases (n=4/5, Fig. 6C, D, F, G). *Lmx1b* expression patterns corresponded to those observed in DorBL and VentBL (Fig. 6E, H, n=8/8 and 5/5, respectively). Furthermore, limb patterning was observed in the dorsal groups (n=12/20) but not in the ventral groups (n=17/17, Fig. 6A, B, lower panels). These findings demonstrate that a straightforward procedure involving dorsal skin wounding and supplementation with BMP2, FGF2, and FGF8 is sufficient to induce accessory limb formation. Remarkably, this method also enabled the induction of multiple limbs within the same limb. Grafting BMP2+FGF2+FGF8-soaked beads to multiple dorsal sites resulted in the formation of multiple limbs along the proximodistal axis (Fig. 6I–L). These results refine our understanding of the role of FGF2 in the ALM, particularly its critical function on the dorsal side.

Discussion

Dorsal and ventral positional cues are required for the induction of Shh expression

In axolotl limb regeneration, cells derived from all four positional origins—anterior, posterior, dorsal, and ventral—are required for an induced blastema to form a limb. This was confirmed through the ALM experiments (Fig. 1). The gene expression patterns in these ALM blastemas revealed distinct molecular characteristics for each group (Fig. 2). *Fgf8* expression in AntBL and *Shh* expression in PostBL are consistent with a previous report (Nacu et al., 2016). The absence of SHH in AntBL and of FGF8 in PostBL likely accounts for their failure to form limbs. *Lmx1b* expression in the dorsal half of both AntBL and PostBL suggests that both dorsal and ventral tissues co-existed in these blastemas (Fig. 2B, G). In contrast, DorBL and VentBL exhibited distinct *Lmx1b* expression patterns, suggesting that most cells in DorBL and VentBL are derived from dorsal or ventral origins, respectively (Fig. 2L, Q). A possible explanation for the lack of *Shh* expression in DorBL and VentBL, despite the expression of *Fgf8* (Fig. 2M, N, R, S), is that the induction of *Shh* expression may depend on the co-existence of dorsal and ventral cells, although *Fgf8* can be expressed independently of the co-existence of dorsal and ventral cells. This idea is supported by the cell-tracing experiment (Fig. 3). In these assays, the posteriorly derived cells expressed *Shh* only when both dorsal and ventral cells were present. These results strongly suggest that the co-existence of dorsal and ventral cells is necessary for inducing *Shh* expression. Consequently, one of the essential roles of the dorsal and ventral positional cues in limb patterning would be inducing *Shh* expression, which facilitates the anteroposterior interaction.

Our findings clarify the hierarchical relationship between dorsal and ventral positional cues and anteroposterior interaction. Our data demonstrate that dorsal and ventral cells are essential for inducing *Shh* expression in a regenerating blastema. Furthermore, we showed that DorBL and VentBL, which typically fail to form a limb, could form patterned limbs with ectopic *Shh* expression, even in the absence of dorsal and ventral cell co-existence (Fig. 4). Furthermore, such limbs exhibited dorsally or ventrally symmetric structures (Fig. 4F, G, J–R), highlighting that dorsoventral patterning depends on the cell origin. Thus, we concluded that dorsal and ventral positional cues are essential for patterned limb formation via inducing *Shh* expression.

WNT10B and FGF2 as dorsal and ventral positional cue molecules

We identified *Wnt10b* and *Fgf2* as candidate genes providing the dorsal and ventral positional cues required to induce *Shh* expression, respectively (Fig. 5). DEG analysis between DorBL and VentBL revealed higher *Wnt10b* expression in DorBL and higher *Fgf2* expression in VentBL (Fig. 5A, B). Supplementation with WNT10B in VentBL and FGF2 in DorBL induced *Shh* expression and subsequent limb patterning (Fig. 5C–G). *Wnt4* expression was also elevated in DorBL, while *Fgf7* and *Tgfb2* were upregulated in VentBL. However, we did not observe *Shh*

327 induction in the *Fgf7*- or *Tgfb2*- electroporated DorBL or in the *Wnt4*-electroporated VentBL. FGF7
328 is known to be capable of inducing the apical ectodermal ridge (AER) in chick limb development
329 (Yonei-Tamura et al., 1999), but little is known about its role in limb regeneration. In newt limb
330 regeneration, KGFR, which acts as FGF7 receptor, is expressed in the basal layer of the wound
331 epithelium, while FGFR1, which acts as FGF2 receptor, is primarily expressed in the mesenchyme
332 (Poulin et al., 1993). This differential expression pattern suggests that FGF2 and FGF7 target distinct
333 cell populations, potentially explaining the differences in their ability to induce *Shh* expression. The
334 difference in the ability of *Wnt10b* and *Wnt4* to induce *Shh* expression in VentBL may be explained
335 by their distinct signaling pathways. WNT10B and WNT4 are typically classified as canonical and
336 non-canonical WNTs, respectively. We observed *Shh* induction in BIO-treated VentBL, indicating
337 that the canonical WNT signaling pathway regulates *Shh* expression. These results support the idea
338 that canonical, but not non-canonical, WNT signaling contributes to *Shh* induction. Regarding *Tgfb2*,
339 TGF-β signaling has been implicated in blastema induction during salamander limb regeneration
340 (Sader and Roy., 2022; Lévesque et al., 2007). However, little is known about the relationship
341 between TGF-β signaling and *Shh* induction in limb development and regeneration, suggesting that
342 TGF-β signaling does not play a primary role in *Shh* induction. Consistent with this, we did not
343 observe *Shh* induction in the *Tgfb2*-electroporated DorBL, as described above. This suggests that
344 TGFB2 signaling may be involved in dorsoventral regulation independent of *Shh* induction. Taken
345 together, among the candidate genes we identified, WNT10B via the canonical WNT pathway and
346 FGF2 via FGFR1 appear to regulate *Shh* induction and the subsequent patterning process.
347 WNT signaling may be the key for the dorsal properties in limb formation. It has been
348 reported that canonical Wnt/β-catenin signaling plays essential roles in limb regeneration among
349 vertebrates, including axolotls (Kawakami et al., 2006; Lovely et al., 2022). In the present study, we
350 demonstrated that introducing *Wnt10b* or BIO treatment could induce *Shh* expression in VentBL,
351 facilitating limb patterning. In mouse limb development, *Wnt10b* is expressed in the apical
352 ectodermal ridge (AER, Witte et al., 2009), and mutations in *Wnt10b* are associated with Split-
353 Hand/Foot Malformation (Ugur and Tolun, 2008; Al Ghamdi et al., 2020; Bilal et al., 2023).
354 However, there is no evidence suggesting that *Wnt10b* contributes to dorsal specificity during limb
355 development. This raises questions about whether the function of *Wnt10b* is unique to axolotls or
356 whether its orthologs in other species might share functional redundancy with other WNT genes.
357 Further studies are needed to clarify this point. Notably, WNT10B utilizes the canonical Wnt
358 signaling pathway, similar to WNT7A, a well-known WNT family gene critical for dorsoventral
359 limb patterning in amniotes. In amniotes, *Wnt7a* is expressed in the dorsal ectoderm of developing
360 limb buds and induces *Lmx1b* expression in dorsal mesenchyme, thereby acting as positional

361 information to establish dorsal characteristics (Riddle et al., 1995; Cygan et al., 1997; Chen, 2002).
362 In axolotls, dorsal-specific *Wnt7a* expression has not been confirmed. Our RNA-seq analysis showed
363 that there was almost no significant difference in *Wnt7a* expression levels between DorBL and
364 VentBL ($\log_2$ (normalized counts) = 5.97, $\log_2$ (fold change) = -0.810, p = 0.401), consistent with
365 previous studies (Shimokawa et al., 2013). These results suggest that *Wnt7a* does not have a dorsal-
366 specific function, at least in axolotl limb regeneration/development. While WNT10B could function
367 as a dorsal positional cue, WNT10B is unlikely to induce dorsal identity, as ectopic *Lmx1b*
368 expression was not observed in *Wnt10b*-introduced VentBL, which formed double-ventral limbs
369 (Fig. 5F–H). This indicates that *Wnt10b* in axolotl limb regeneration does not simply replace the
370 function of *Wnt7a* in amniote limb development. Nevertheless, the involvement of canonical WNT
371 signaling in dorsal function and limb morphogenesis remains an important area for further
372 investigation.
373 We identified FGF2 as the ventral positional cue, which plays a crucial role in limb
374 patterning process in axolotl limb regeneration. This aligns with previous studies showing that *Fgf2*
375 expression correlates with limb regeneration in salamanders (Giampaoli et al., 2003). *Fgf2*
376 expression was relatively high in VentBL, and *Fgf2*-introduced DorBL formed patterned limbs (Fig.
377 5). These results indicate that FGF2 supplementation can substitute for the presence of ventral cells
378 in the limb patterning process. It is noteworthy that FGF2 application does not appear to induce
379 ventral identity, as the limbs formed from *Fgf2*-introduced DorBL exhibited dorsally symmetric limb
380 structures. The finding that FGF signaling functions in dorsoventral control is not a well-known
381 mechanism across species studied to date. Whether this represents an axolotl-specific regulatory
382 mechanism or a broader function of FGF signaling in limb morphogenesis remains to be determined.
383 Our findings suggest that although WNT10B and FGF2 act as dorsal and ventral positional
384 cues, they do not affect dorsal or ventral identities. In amniote limb development, WNT7A functions
385 as dorsal "positional information" by inducing dorsal identity through *Lmx1b* expression. In contrast,
386 in axolotls, supplementation with WNT10B in VentBL or FGF2 in DorBL did not affect the
387 expression patterns of *Lmx1b* (Fig. 5C). Moreover, the limbs formed from such DorBL and VentBL
388 exhibited dorsally and ventrally symmetric structures (Fig. 5F–H). These findings suggest that
389 dorsoventral identities in axolotls are not affected by WNT10B or FGF2 supplementation. Thus, in
390 the present study, we used the term "positional cue" to distinguish this role from "positional
391 information," which provides positional identities. We previously reported that the expression
392 patterns of *Lmx1b* in axolotl limb regeneration are likely to depend on the positional origins of cells
393 (Iwata et al., 2020; Yamamoto et al., 2022). The identities of cells along the dorsoventral axis may be
394 controlled by their positional memory and determined before the initiation of limb regeneration.

395 The present study revealed that the dorsal and ventral positional cue molecules WNT10B
396 and FGF2 regulate *Shh* expression during limb patterning in axolotls. These findings highlight a
397 degree of conservation between axolotl limb regeneration and amniote limb development. In
398 amniote limb development, FGF and WNT signaling pathways are key regulators of *Shh* expression.
399 In developing amniote limb buds, *Fgf2* is expressed in the ectoderm, including AER and adjacent
400 mesoderm, mediating distal outgrowth. FGFs, including FGF2, from AER are known to maintain
401 *Shh* expression (Laufer et al., 1994; Niswander et al., 1994; Yang and Niswander, 1995; Li et al.,
402 1996). Similarly, WNT7A regulates *Shh* expression in amniote limb development, and loss of
403 WNT7A function results in reduced *Shh* expression in the zone of polarizing activity (ZPA) and the
404 deletion of posterior structures (Parr and McMahon, 1995). Thus, our findings provide new insights
405 into the conserved and divergent roles of dorsal-ventral signaling in regulating *Shh* expression,
406 furthering our understanding of limb morphogenesis.
407
408 ***The integration mechanism of the four positional cues***
409 In the present study, we reveal the molecular hierarchy of the four positional cues—
410 anterior, posterior, dorsal, and ventral—in axolotl limb regeneration and explain how these positional
411 cues are integrated to form a patterned limb (Fig 7). In our proposed model, following amputation,
412 nerves first trigger blastema induction by secreting nerve factors, such as BMP and FGFs (Makanae
413 et al., 2014, Satoh et al., 2016). These nerve factors stimulate connective tissue cells, including
414 dermal cells, to generate multipotent mesenchymal blastemal cells (Muneoka et al., 1986; Kragl et
415 al., 2009; Hirata et al., 2010; Gerber et al., 2018). Simultaneously, *Wnt10b* and *Fgf2* are expressed at
416 higher levels in dorsal and the ventral blastemal cells, respectively. In the next phase, the co-
417 existence of WNT10B and FGF2 induces *Shh* expression in the posterior region of the blastema.
418 During this phase, *Fgf8* is expressed in the anterior mesenchyme independently of the co-existence
419 of dorsal and ventral cells (Fig. 7A). These expression patterns of *Wnt10b*, *Fgf2*, *Shh*, and *Fgf8* may
420 be determined by the positional memory of cells (Otsuki et al., 2021). In the subsequent phase, the
421 anteroposterior interaction, mediated by FGF8 and SHH, supports distal outgrowth to form a limb.
422 This model explains previous observations in studies on double-half limbs and ALM blastemas
423 (AntBL, PostBL, DorBL, and VentBL), which typically fail to form a limb. In blastemas induced
424 from double-anterior and double-posterior limbs, or AntBL (Fig. 7B) and PostBL (Fig. 7C), SHH or
425 FGF8 proteins are likely absent due to the lack of anteriorly or posteriorly derived cells. Similarly, in
426 blastemas induced by amputating double-dorsal and double-ventral limbs, or DorBL (Fig. 7D) and
427 VentBL (Fig. 7E), FGF2 or WNT10B proteins are likely absent or insufficient because of the lack of
428 ventrally or dorsally derived cells. This results in the absence of SHH, even if posteriorly derived

429 cells are present. In all these cases, the absence of either FGF8 or SHH disrupts the anteroposterior
430 interaction, leading to failure in limb patterning. We concluded that the requirement for cells derived
431 from all four positional origins is underpinned by this integration model. In this model, dorsal and
432 ventral positional cues activate the posterior positional cue, enabling mutual interaction with the
433 anterior cue. This interplay ensures proper anteroposterior interaction and complete limb patterning.
434
435

436 ## *Materials and Methods*

437 ### *Animal procedures*

438 Axolotls between 4 and 15 cm from snout to tail tip were housed in tap water at 22°C. Both
439 forelimbs and hind limbs were used for surgical procedures without distinction. Transgenic axolotls
440 were obtained from the Ambystoma Genetic Stock Center (http://www.ambystoma.org/genetic-
441 stock-center). Animals were anesthetized in 0.1% MS222 (Sigma-Aldrich) solution before surgical
442 procedures.

443 In the ALM experiments, skin was peeled from the anterior, posterior, dorsal, or ventral
444 side of a limb at the stylopod level, so that the skin of the opposite side was not injured. Thus, the
445 size of the injured area depended on the limb size. Then, thick bundles of nerve trunks running the
446 center of a limb was deviated the injured region. For the cell-tracing experiment, a piece of posterior
447 half of the dorsal or ventral skin was obtained from GFP-expressing transgenic animals and grafted
448 to the ALM region.

449 Protein-soaked beads for grafting were prepared as previously described (Makanae et al.,
450 2014; Kashimoto et al., 2023). In brief, air-dried gelatin beads were allowed to swell in stock
451 solution (1 μg/μL) prepared following the manufacturer's instructions. Equal amounts of proteins
452 were used when formulating the combination protein mixture. Beads were soaked in the mixture of
453 proteins (Bmp2 [mouse], Fgf2 [mouse], and Fgf8 [human/mouse]; R&D Systems) overnight at 4°C.
454 For control experiments, gelatin beads were soaked in DDW. Before grafting, dorsal or ventral skin
455 was peeled because full-thickness skin inhibits limb regeneration (Thornton, 1962; Mescher, 1976;
456 Tsai, 2020). The beads were grafted under the wounded epidermis at 3 dps. The limbs were fixed 10
457 days after grafting. The details of grafting procedures are as previously described (Makanae et al.,
458 2014; Kashimoto et al., 2023).

459 To analyze skeletal patterns, induced limbs were stained with alcian blue and alizarin red.
460 Samples were fixed in 100% ethanol for 1 day at room temperature, then stained with Alcian blue
461 solution (Wako, pH 2.0) in 20% acetic acid (Nacalai Tesque) with 80% ethanol solution at 37°C
462 overnight. Then, samples were washed in tap water several times and fixed in 10% Formaldehyde
463 Neutral Buffer Solution (Nacalai Tesque) for 1 day. Samples were then stained with Alizarin red S
464 (Nacalai Tesque) in the solution (4% KOH:10% Formaldehyde Neutral Buffer Solution = 2:3) at
465 room temperature for 1 day. Finally, samples were placed in graded glycerol with 4% KOH for
466 clearing.

467 For BIO treatment, 10 mM stock solution of 6-bromoindirubin-3-oxime (BIO, Selleck,
468 S7198) dissolved in DMSO was stored in the dark at 4°C. Axolotls soon after surgery were raised in
469 tap water with BIO solution (experimental) or with the same amount of solvent, DMSO (control),
470 until 14 dps for qPCR and 30 dps for phenotype analysis. The containers including water and
471 axolotls were kept in the dark during BIO or DMSO treatment. For BIO treatment, axolotls between

472 4 and 5 cm from snout to tail tip were used.
473
474 ***Sectioning and histological staining***
475 Samples were fixed in 4% PFA/PBS overnight at room temperature before sectioning. The fixed
476 samples were embedded in O.C.T. compound (Sakura) following 30% sucrose/PBS treatment for
477 approximately 12 h at 4°C. Frozen sections of 14 μm thickness were prepared using Leica CM1850
478 (Nussloch). The sections were well dried under an air dryer and kept at -80°C until use.
479 Standard hematoxylin and eosin (HE) staining and Masson's trichrome staining were used
480 for histological analysis. To visualize cartilage formation, Alcian blue staining was performed before
481 HE staining. In brief, sections were washed in tap water several times to remove the O.C.T.
482 compound. Then, the sections were stained with Alcian blue (Wako, pH 2.0), and then HE staining
483 was performed. Trichrome stain (Masson) kit (Sigma, HT15-1KT) was used for trichrome staining.
484 The stained sections were mounted using Softmount (Wako).
485
486 ***In situ hybridization***
487 *In situ* hybridization was performed as described previously (Yamamoto et al., 2022). For probe
488 synthesis, target genes cloned on pTAC-2 plasmid (BioDynamics Lab Inc.) were amplified by PCR
489 using M13 primers. PCR fragments were purified and used as an RNA probe template. RNA probe
490 synthesis was performed with Sp6 RNA polymerase (Takara) for 3 h, and RNA was hydrolyzed for
491 11 min. The sections were washed in PBT to remove the O.C.T. compound, treated with proteinase
492 K (10 μg/mL) (Invitrogen)/PBT for 20 min at room temperature, washed in PBT, treated with 4%
493 PFA/PBS for 20 min at room temperature, washed in PBT, and then probes were hybridized at
494 62.5°C for approximately 18 h. The sections were washed in wash buffer 1 (formamide:H_2O:20×
495 SSC [3M NaCl:0.3M sodium citrate, pH 5.0] = 2:1:1), and then in wash buffer 2
496 (formamide:H_2O:20× SSC = 5:1:4). The samples were then incubated with anti-digoxigenin-AP Fab
497 fragments (Sigma-Aldrich, 1/1000) for 2 h at room temperature. Samples were stained with BCIP
498 (Nacalai Tesque) and NBT (Nacalai Tesque) in alkaline phosphatase buffer (0.1M NaCl, 0.1M Tris-
499 HCl [pH9.5], 0.1% Tween20) for 18 h at room temperature after washing in TBST.
500
501 ***Immunofluorescence***
502 Immunofluorescence on sections was carried out based on a previous report (Yamamoto et al.,
503 2022). The antibodies were as follows: anti-GFP (MBL, #598, 1/500), anti-acetylated alpha tubulin
504 (Santa Cruz, #sc-23950, 1/1000), anti-mouse IgG Alexa 488 (Invitrogen, #A11017, 1/1000), anti-
505 rabbit IgG Alexa 488 (Invitrogen, #A21206, 1/500). Nuclei were stained with Hoechst (Nacalai
506 Tesque), and images were captured using an Olympus BX51 system.

507

508 ***RNA-Seq analysis***

509 Total RNA was extracted from DorBL and VentBL at 10 dps using TriPure reagent (Roche),
510 following the manufacturer's instructions. Three biological replicates were prepared for both
511 samples. 150 bp paired-end RNA-seq reads were obtained under contract to Rhelixa (Tokyo, Japan),
512 using Illumina Nova Seq 6000 and SMART-Seq HT Plus Kit (#R400449). RNA-seq data were
513 analyzed on Galaxy (https://usegalaxy.eu/root) as follows. Sequence reads were trimmed and the
514 quality was filtered by Trimmomatic v0.39 (Bolger et al., 2014) with the following parameters
515 (LEADING:20, TRAILING:20, SLIDINGWINDOW:4:15, MINLEN:36). Axolotl genome data
516 (AmexG_v6.0-DD) and annotation data (AmexT_v47-AmexG_v6.0-DD.gtf) were obtained from
517 AXOLOTL-OMICS (https://www.axolotl-omics.org/) (Schloissnig et al., 2021). Mapping to the
518 Axolotl genome (AmexG_v6.0-DD) was performed with HISAT2 v2.2.1 (Kim et al., 2015). Count
519 data were obtained with featureCounts v2.0.8 (Liao et al., 2013) on the basis of the Axolotl gene
520 model (AmexT_v47-AmexG_v6.0-DD.gtf). DEGs were identified with DESeq2 v2.11.40.8 (Love et
521 al., 2014) ($p < 0.05$). Among identified DEGs (DorBL > VentBL; 762 genes, VentBL > DorBL; 513
522 genes), genes annotated as "intercellular signaling molecule" were explored on PANTHER
523 (https://www.pantherdb.org/) (Thomas et al., 2003), and 21 genes (DorBL > VentBL; 5 genes,
524 VentBL > DorBL; 16 genes) were identified as candidate genes of dorsal and ventral positional cues,
525 as shown below:

526

527 DorBL > VentBL:

528 WNT4 (AMEX60DD052091), WNT10B (AMEX60DD029981), SEMA3A (AMEX60DD023165),
529 LECT2 (AMEX60DD041044), ANGPTL5 (AMEX60DD049512).

530

531 VentBL > DorBL:

532 FCN1 (AMEX60DD050926), CXCL14 (AMEX60DD028973), DNER (AMEX60DD002010),
533 FGF7 (AMEX60DD003767), CXCL12 (AMEX60DD052412), CXCL8 (AMEX60DD044133),
534 SEMA6A (AMEX60DD042813), ANGPTL2 (AMEX60DD050490), ANGPTL6
535 (AMEX60DD031854), FGL2 (AMEX60DD006387), VWDE (AMEX60DD022491), TGFB2
536 (AMEX60DD036126), FGF2 (AMEX60DD044865), EFNA4 (AMEX60DD014882), EFNA3
537 (AMEX60DD014867), ANGPTL1 (AMEX60DD018261).

538

539 ***Cloning candidate genes and preparation of construct vectors for overexpression***

540 Among the identified candidate genes, we focused on *Wnt10b*, *Wnt4*, *Fgf2*, *Fgf7*, and *Tgfb2*. We
541 cloned these genes in pTAC-2 plasmids from cDNA obtained from blastemas. The following primers

542 were used:
543
544 Wnt10b Fwd:ATGGCCCACAGCTCACCCTCCGACACC
545 Wnt10b Rev:TCACTTGCACACATTCACCCATTCTGTG
546 Wnt4 Fwd:ATGGATGCTCACGAAAGCAGCGTATATC
547 Wnt4 Rev:TCACCGGCAGGTGTGCATTTCTACCAC
548 Fgf2 Fwd:ATGGCGGCGGGGAGCATCACCACCTTGC
549 Fgf2 Rev:TCAACTCTTGGCCGACATGGGAAGGAAAAG
550 Fgf7 Fwd:ATGCGCAGATGGGTGCTAGCTTGGATC
551 Fgf7 Rev:TCATGTGTTATTGGATATACGCATTGGA
552 TGFB2 Fwd:ATGAGATTACAATTACTGAGAAAAAAAATG
553 TGFB2 Rev:TTAGCTGCACTTGCAAGATTTTACAATCA
554
555 We then inserted these genes to p2a-AcGFP-pCS2 vectors with In-Fusion® HD Cloning Kit
556 (Clontech). The following primers were used for PCR before In-Fusion reaction:
557
558 pCS2 inverse Fwd:GCTACTAACTTCAGCCTGCTGAAGCAGG
559 pCS2 inverse Rev:CATCGATGGGATCCTGCAAAAAGAACAAGTAGCTT
560 Wnt10b Fwd:AGGATCCCATCGATGGCCCACAGCTCACCCTCCGA
561 Wnt10b Rev:GCTGAAGTTAGTAGCCTTGCACACATTCACCCA
562 Wnt4 Fwd:AGGATCCCATCGATGGATGCTCACGAAAGCAGCG
563 Wnt4 Rev:GCTGAAGTTAGTAGCCCGGCAGGTGTGCATTTCTA
564 Fgf2 Fwd:AGGATCCCATCGATGGCGGCGGGGAGCATCACCA
565 Fgf2 Rev:GCTGAAGTTAGTAGCACTCTTGGCCGACATGGGAA
566 Fgf7 Fwd:AGGATCCCATCGATGCGCAGATGGGTGCTAGCTTG
567 Fgf7 Rev:GCTGAAGTTAGTAGCTGTGTTATTGGATATACGCA
568 Tgfb2 Fwd:AGGATCCCATCGATGAGATTACAATTACTGAGAAA
569 Tgfb2 Rev:GCTGAAGTTAGTAGCGCTGCACTTGCAAGATTTTA
570
571 Finally, the following DNA constructs were obtained; *Wnt10b*-p2a-GFP (pCS2), *Wnt4*-p2a-GFP
572 (pCS2), *Fgf2*-p2a-GFP (pCS2), *Fgf7*-p2a-GFP (pCS2), and *Tgfb2*-p2a-GFP (pCS2).
573
574 ***Electroporation***
575 Each DNA construct was injected directly into the target region. Immediately after injection, electric
576 pulses were applied (20 V, 50 ms pulse length, 950 ms interval, 10 times) with NEPA21(Nepa gene).
577 The injected DNA constructs were as follows: pCS2-AcGFP, pCS2-*Shh*-p2a-AcGFP, *Wnt10b*-p2a-

578 GFP (pCS2), *Wnt4*-p2a-GFP (pCS2), *Fgf2*-p2a-GFP (pCS2), *Fgf7*-p2a-GFP (pCS2), and *Tgfb2*-p2a-
579 GFP (pCS2). All plasmids were purified using a Genopure Maxi kit (Roche). Electroporation was
580 performed at -3, 4, and 7 dps and samples were fixed at 10 dps for *in situ* hybridization. To analyze
581 the phenotype of 90 dps samples, electroporation was performed at -3, 4, 7, 10, 15, 20, 25, and 30
582 dps.
583
584 ***qRT-PCR***
585 The procedures of qRT-PCR were previously described (Yamamoto et al., 2022). In brief, RT was
586 performed using Prime Script II (Takara), and qPCR was performed using KAPA SYBR FAST
587 qPCR Master Mix (Kapa Biosystems) and StepOne (ThermoFisher Scientific). Primers were as
588 follows:
589
590 Ef-1α Fwd: AACATCGTGGTCATCGGCCAT
591 Ef-1α Rev: GGAGGTGCCAGTGATCATGTT
592 Shh Fwd: GCTCTGTGAAAGCAGAGAACTCG
593 Shh Rev: CGCTCCGTCTCTATCACGTAGAA
594
595 RNA for Fig. 5D was prepared from FGF2- or DDW-soaked bead grafted DorBL. Bead grafting was
596 performed at 7 dps and RNA preparation was performed at 14 dps. RNA for Fig. 5E was prepared
597 from 1μM BIO- or DMSO-treated VentBL at 14 dps. *Ef-1α* was used as the internal control. We
598 conducted a two-tailed Welch's *t*-test for statistical analysis.
599
600 ***Pixel classification and calculating symmetry scores***
601 A machine learning-based method was applied for pixel classification using ilastic software
602 (downloaded on https://www.ilastik.org/). The details and workflows were previously described
603 (Berg et al., 2019). Each pixel in the images was classified into five classes. The regions of the
604 background (Class 1), cartilage (Class 2), muscle (Class 3), other connective tissue (Class 4), and
605 epidermis (Class 5) were annotated for training data. Using these annotated regions as references,
606 pixels were automatically classified into the respective classes. In this process, the same training data
607 were used for images obtained from the same limb. Then, symmetry scores were calculated for each
608 class individually and for the combined set of all classes. In this process, the external shape of the
609 section, which could bend randomly during sample fixation process, would affect the symmetry
610 scores if the entire region were used. To focus on the symmetry of the anatomical patterns, images
611 with 400 μm width were prepared (Fig. 4L, 5E, F). The symmetry scores of pixel-classified images
612 were calculated using python. First, the center of the dorsal end and ventral end was set as the axis of

symmetry. Then, one side of the image was flipped. Next, color masks were generated for both sides of the image. These masks identified pixels that matched the specified color. Pixels were considered to match if their RGB values were within the given tolerance range for all three channels. In pixel comparison, the masks for one side and the other side were compared to calculate the following pixels:

Matching pixels: The number of pixels that match in both sides for the specified color.
Total pixels: The total number of pixels matching the color in either side.

The symmetry scores were computed as (Number of Matching Pixels)/(Total Pixels in Both Sides). The scores were obtained from 12 areas of each group. For statistical analysis, a two-tailed a two-tailed Welch's *t*-test was used. In this analysis, each group was compared to the intact limb group because the intact limb should be set as a typical asymmetrical structure.

Author contributions

Conceptualization: S.Y., A.S.; Methodology: S.Y., M.H., A.S; Validation: S.Y.; Formal analysis: S.Y.; Investigation: S.Y.; Resources: S.Y., S.F., A.O., A.S.; Data curation: S.Y.; Writing - original draft: S.Y.; Writing - review & editing: S.Y., S.F., A.O., M.H., A.S.; Visualization: S.Y., A.S.; Supervision: A.S.; Project administration: A.S.; Funding acquisition: A.S., S.Y.

Acknowledgments

We are grateful to R. Iwata and T. Satoh for supporting office work and animal housing. Animals were obtained through Hiroshima University Amphibian Research Center. This work is supported by the Japan Society for the Promotion of Science KAKENHI grant-in-aid for scientific research (B) (20H03264 and 24K02034 to A.S.) and by a Grant-in-Aid for Japan Society for the Promotion of Science fellows (24KJ1718 to S.Y.).

642 ***Figure Legends***

643 ***Figure 1. ALM experiments at the four positions.***

644 (A) Schematic image of anatomy at the stylopod level of axolotl limb. HE staining (bright field) and
645 acetylated alpha tubulin, visualized by immunofluorescence (green, dark field), are shown in the
646 right panels. Black and white arrows, respectively, indicate major blood vessels and nerves. H:
647 *humerus*, AHL: *Anconaeus humeralis lateralis*, HAB: *Humeroantebrachialis*, CBL:
648 *coracobrachialis longus*. (B–I) Blastemas induced at the anterior, posterior, dorsal, or ventral region
649 by skin wounding plus nerve deviation without (B–E) or with (F–I) skin grafting from the opposite
650 side of the limb. Images were captured at 10 and 60 dps. Scale bar = 3 mm.

651

652 ***Figure 2. Gene expression patterns of the ALM-induced blastemas.***

653 Sections of anteriorly (A–D), posteriorly (F–I), dorsally (K–N), or ventrally (P–S) induced blastemas
654 at 10 dps. Acetylated alpha tubulin (A–P) was visualized by immunofluorescence. Expression of
655 *Lmx1b* (B–Q), *Fgf8* (C–R), and *Shh* (D–S) in the regions indicated by white boxes in (A–P) was
656 visualized by *in situ* hybridization. Black and white arrowheads indicate the signals of *Fgf8* and *Shh*
657 expression, respectively. The dotted line indicates the epithelial-mesenchyme border. (E–T)
658 Schematic images of gene expression patterns. Scale bar = 700 μm.

659

660 ***Figure 3. Co-existence of dorsal and ventral cells induces Shh expression.***

661 (A) Experimental scheme. Posterior half of dorsal (PD_{gfp}) or ventral (PV_{gfp}) GFP-expressing
662 skin was grafted on VentBL (VentBL+PD_{gfp}; C, D / VentBL+PV_{gfp}; G, H), or DorBL
663 (DorBL+PD_{gfp}; E, F / DorBL+PV_{gfp}; I, J) region. (B) Induced blastemas at 10 dps; images of
664 bright and dark fields are merged. (C–J) Dark and bright fields of the same sections of induced
665 blastemas at 10 dps. Red boxes in (C–I) indicate the corresponding regions of lower images.
666 Expressions of *Shh* and *Lmx1b* were visualized by *in situ* hybridization. GFP signals were visualized
667 by immunofluorescence. Arrowheads indicate the cells expressing *Shh*. The dotted line indicates the
668 epithelial-mesenchyme border. Scale bar = 3 mm (B) and 700 μm (C).

669

670 ***Figure 4. Limb formation without the co-existence of dorsal and ventral cells by SHH***
671 ***supplementation.***

672 (A) Experimental scheme. *Shh*-p2A-GFP- or GFP-containing pCS2 vector was electroporated (EP)
673 into AntBL, DorBL, and VentBL. (B) Induced blastemas at 14 dps; images of bright and dark
674 fields are merged. (C–G) Phenotypes at 90 dps. (H–K) Histological analysis of intact and induced
675 limbs. Standard Masson's trichrome staining was performed on the transverse sections. The dotted
676 boxes indicate the regions shown in (L). (L) Upper panels: analyzed regions for calculating
677 symmetry scores. Lower panels: images after pixel classification by machine learning. (C–I)

678 Symmetry scores of each class. Scores obtained from the same limb are plotted at the same x-
679 coordinates. n.s.; no significant difference, *p<0.05, **p<0.005. Scale bar = 2 mm (B), 4 mm (C–
680 G), and 1 mm (H–K).
681
682 ***Figure 5. Identification of candidate molecules of the dorsal and ventral positional cues.***
683 RNA-Seq was performed on DorBL and VentBL at 10 dps. (A) MA plot of the result. (B) List of
684 DEGs annotated as "intercellular signaling molecules." (C) Bright and dark fields of sections of
685 DorBL and VentBL at 10 dps with candidate genes introduced. Expression of *Shh* and *Lmx1b* was
686 visualized by *in situ* hybridization, and GFP signals were visualized by immunofluorescence.
687 Arrowheads indicate the cells expressing *Shh*. The white boxes indicate the regions of the lower
688 panels. Images of dark and bright fields of *Shh* are obtained from the same section. (D, E)
689 Quantitative analysis of *Shh* expression in DorBL with FGF2-soaked bead and with DDW-soaked
690 bead (D) and in VentBL treated with 1μM BIO and with DMSO (E). RNA was prepared from 8
691 identical DorBL for both (D) and from 4 identical VentBL for both (E). Technological replicates are
692 plotted in the same color. (F, G) The limbs formed from VentBL with *Wnt10b* and DorBL with *Fgf2*
693 at 90 dps. Histological analysis and pixel classification was performed in the same way as in Fig. 4.
694 The dotted boxes indicate the regions shown in the right panels. (H) Symmetry scores of each class.
695 Scores obtained from the same limb are plotted at the same x-coordinates. The plots of "int" are the
696 same plots as in Fig. 4. n.s.; no significant difference, *p<0.05, **p<0.005. Scale bar = 700 μm (C),
697 4 mm (F, G, upper panels), 1 mm (F, G, lower panels).
698
699 ***Figure 6. Limb formation at the dorsal region by BMP2+FGF2+FGF8 supplementation.***
700 (A, B) 14 and 60 dps phenotypes of BMP2+FGF2+FGF8 supplementation by bead grafting at the
701 dorsal (A) or ventral (B) region. Neither nerve deviation nor skin grafting was performed. (C–H)
702 Expression patterns of *Fgf8*, *Shh* and *Lmx1b* of induced blastemas at 10 dps. Expression was
703 visualized by *in situ* hybridization. The dotted line indicates the external shape of the blastema. (I–
704 K) Phenotype obtained by BMP2+FGF2+FGF8 supplementation to two dorsal regions of an
705 identical limb. (L) Phenotype obtained by BMP2+FGF2+FGF8 supplementation to five dorsal
706 regions of an identical limb. Scale bar = 3 mm (B), 700 μm (H), 2 cm (J), 1 cm (K, L).
707
708 ***Figure 7. The integration model of the four positional cues.***
709 Schematic images of a normal blastema (A), AntBL (B), PostBL (C), DorBL (D), and VentBL (E).
710 Green, red, blue, and yellow boxes within the blastema represent cells derived from anterior,
711 posterior, dorsal, and ventral regions, respectively. Colored arrows indicate the presence of the

corresponding positional cue molecules. In this model, limb patterning requires both FGF8 and SHH, and *Shh* expression in posteriorly derived cells is induced by the co-existence of WNT10B and FGF2.

Figure S1. Limb patterning from BIO-treated VentBL.

(A, B) VentBL treated with 1μM BIO (A) or DMSO (B) at 90 dps. (C–D) Histological analysis and pixel classification was performed in the same way as in Fig. 4. The dotted boxes indicate the regions shown in (D). (E) Symmetry scores of each class. Scores obtained from the same limb are plotted at the same x-coordinates. The plots of "int" are the same plots as in Fig. 4. n.s.; no significant difference, *$p<0.05$, **$p<0.005$. Scale bar = 4 mm (B), 1 cm (C).

Table 1. The induction rate of bump/limb formation in ALM.

References

Al Ghamdi, M. A., Al-Qattan, M. M., Hadadi, A., Alabdulrahman, A., Almuzzaini, B., Alatwi, N., & AlBalwi, M. A. (2020). A classification system for split-hand/ foot malformation (SHFM): A proposal based on 3 pedigrees with WNT10B mutations. European Journal of Medical Genetics, 63(3), 103738. https://doi.org/https://doi.org/10.1016/j.ejmg.2019.103738

Berg, S., Kutra, D., Kroeger, T., Straehle, C. N., Kausler, B. X., Haubold, C., Schiegg, M., Ales, J., Beier, T., Rudy, M., Eren, K., Cervantes, J. I., Xu, B., Beuttenmueller, F., Wolny, A., Zhang, C., Koethe, U., Hamprecht, F. A., & Kreshuk, A. (2019). ilastik: interactive machine learning for (bio)image analysis. Nature Methods, 16(12), 1226–1232. https://doi.org/10.1038/s41592-019-0582-9

Bilal, M., Haack, T. B., Buchert, R., Peralta, S., Ahmad, I., Faisal, Abbasi, S., & Ahmad, W. (2023). Sequence Variants in the WNT10B Underlying Non-Syndromic Split-Hand/Foot Malformation. Molecular Syndromology, 14(6), 469–476. https://doi.org/10.1159/000531069

Bolger, A. M., Lohse, M., & Usadel, B. (2014). Trimmomatic: a flexible trimmer for Illumina sequence data. Bioinformatics, 30(15), 2114–2120. https://doi.org/10.1093/bioinformatics/btu170

BRYANT, S. V. (1976). Regenerative failure of double half limbs in Notophthalmus viridescens. Nature, 263(5579), 676–679. https://doi.org/10.1038/263676a0

Bryant, S. V, & Baca, B. A. (1978). Regenerative ability of double-half and half upper arms in the newt, Notophthalmus viridescens. Journal of Experimental Zoology, 204(3), 307–323. https://doi.org/https://doi.org/10.1002/jez.1402040302

Bryant, S. V, & Iten, L. E. (1976). Supernumerary limbs in amphibians: Experimental production in Notophthalmus viridescens and a new interpretation of their formation. Developmental Biology, 50(1), 212–234. https://doi.org/https://doi.org/10.1016/0012-1606(76)90079-8

Burton, R., Holder, N., & Jesani, P. (1986). The regeneration of double dorsal and double ventral limbs in the axolotl. Development, 94(1), 29–46. https://doi.org/10.1242/dev.94.1.29

Chen H, J. R. (2002). Interactions between dorsal-ventral patterning genes lmx1b, engrailed-1 and wnt-7a in the vertebrate limb. Int J Dev Biol, 46(7), 937–941.

Chen, H., Lun, Y., Ovchinnikov, D., Kokubo, H., Oberg, K. C., Pepicelli, C. V, Can, L., Lee, B., & Johnson, R. L. (1998). Limb and kidney defects in Lmx1b mutant mice suggest an involvement of LMX1B in human nail patella syndrome. Nature Genetics, 19(1), 51–55. https://doi.org/10.1038/ng0598-51

Cygan, J. A., Johnson, R. L., & McMahon, A. P. (1997). Novel regulatory interactions revealed by studies of murine limb pattern in Wnt-7a and En-1 mutants. Development, 124(24), 5021–5032. https://doi.org/10.1242/dev.124.24.5021

Endo, T., Bryant, S. V, & Gardiner, D. M. (2004). A stepwise model system for limb regeneration. Developmental Biology, 270(1), 135–145.

https://doi.org/https://doi.org/10.1016/j.ydbio.2004.02.016

Endo, T., Gardiner, D. M., Makanae, A., & Satoh, A. (2015). The Accessory Limb Model: An Alternative Experimental System of Limb Regeneration. In A. Kumar & A. Simon (Eds.), Salamanders in Regeneration Research: Methods and Protocols (pp. 101–113). Springer New York. https://doi.org/10.1007/978-1-4939-2495-0_8

Gerber, T., Murawala, P., Knapp, D., Masselink, W., Schuez, M., Hermann, S., Gac-Santel, M., Nowoshilow, S., Kageyama, J., Khattak, S., Currie, J. D., Camp, J. G., Tanaka, E. M., & Treutlein, B. (2018). Single-cell analysis uncovers convergence of cell identities during axolotl limb regeneration. Science, 362(6413), eaaq0681. https://doi.org/10.1126/science.aaq0681

Giampaoli, S., Bucci, S., Ragghianti, M., Mancino, G., Zhang, F., & Ferretti, P. (2003). Expression of FGF2 in the limb blastema of two Salamandridae correlates with their regenerative capability. Proceedings of the Royal Society of London. Series B: Biological Sciences, 270(1530), 2197–2205. https://doi.org/10.1098/rspb.2003.2439

Hirata, A., Gardiner, D. M., & Satoh, A. (2010). Dermal fibroblasts contribute to multiple tissues in the accessory limb model. DGD, 52(4), 343–350. https://doi.org/https://doi.org/10.1111/j.1440-169X.2009.01165.x

Iten, L. E., & Bryant, S. V. (1975). The interaction between the blastema and stump in the establishment of the anterior-posterior and proximal-distal organization of the limb regenerate. Developmental Biology, 44(1), 119–147. https://doi.org/https://doi.org/10.1016/0012-1606(75)90381-4

Iwata, R., Makanae, A., & Satoh, A. (2020). Stability and plasticity of positional memory during limb regeneration in Ambystoma mexicanum. Developmental Dynamics, 249(3), 342–353. https://doi.org/https://doi.org/10.1002/dvdy.96

Kashimoto, R., Furukawa, S., Yamamoto, S., & Satoh, A. (2023). Bead Implantation and Delivery of Exogenous Growth Factors. In A. W. Seifert & J. D. Currie (Eds.), Salamanders: Methods and Protocols (pp. 209–216). Springer US. https://doi.org/10.1007/978-1-0716-2659-7_14

Kawakami, Y., Rodriguez Esteban, C., Raya, M., Kawakami, H., Martí, M., Dubova, I., & Izpisúa Belmonte, J. C. (2006). Wnt/β-catenin signaling regulates vertebrate limb regeneration. Genes & Development, 20(23), 3232–3237. https://doi.org/10.1101/gad.1475106

Kim, D., Langmead, B., & Salzberg, S. L. (2015). HISAT: a fast spliced aligner with low memory requirements. Nature Methods, 12(4), 357–360. https://doi.org/10.1038/nmeth.3317

Kragl, M., Knapp, D., Nacu, E., Khattak, S., Maden, M., Epperlein, H. H., & Tanaka, E. M. (2009). Cells keep a memory of their tissue origin during axolotl limb regeneration. Nature, 460(7251), 60–65. https://doi.org/10.1038/nature08152

Laufer, E., Nelson, C. E., Johnson, R. L., Morgan, B. A., & Tabin, C. (1994). Sonic hedgehog and Fgf-4 act through a signaling cascade and feedback loop to integrate growth and patterning of the

developing limb bud. Cell, 79(6), 993–1003. https://doi.org/https://doi.org/10.1016/0092-8674(94)90030-2

Lévesque, M., Gatien, S., Finnson, K., Desmeules, S., Villiard, É., Pilote, M., Philip, A., & Roy, S. (2007). Transforming Growth Factor: β Signaling Is Essential for Limb Regeneration in Axolotls. PLOS ONE, 2(11), e1227-. https://doi.org/10.1371/journal.pone.0001227

Li, S., Anderson, R., Reginelli, A. D., & Muneoka, K. (1996). FGF-2 influences cell movements and gene expression during limb development. Journal of Experimental Zoology, 274(4), 234–247. https://doi.org/https://doi.org/10.1002/(SICI)1097-010X(19960301)274:4<234::AID-JEZ4>3.0.CO;2-Q

Liao, Y., Smyth, G. K., & Shi, W. (2014). featureCounts: an efficient general purpose program for assigning sequence reads to genomic features. Bioinformatics, 30(7), 923–930. https://doi.org/10.1093/bioinformatics/btt656

Love, M. I., Huber, W., & Anders, S. (2014). Moderated estimation of fold change and dispersion for RNA-seq data with DESeq2. Genome Biology, 15(12), 550. https://doi.org/10.1186/s13059-014-0550-8

Lovely, A. M., Duerr, T. J., Qiu, Q., Galvan, S., Voss, S. R., & Monaghan, J. R. (2022). Wnt Signaling Coordinates the Expression of Limb Patterning Genes During Axolotl Forelimb Development and Regeneration. Frontiers in Cell and Developmental Biology, 10. https://www.frontiersin.org/journals/cell-and-developmental-biology/articles/10.3389/fcell.2022.814250

Maden, M. (1980). Structure of supernumerary limbs. Nature, 286(5775), 803–805. https://doi.org/10.1038/286803a0

Makanae, A., Mitogawa, K., & Satoh, A. (2014). Co-operative Bmp- and Fgf-signaling inputs convert skin wound healing to limb formation in urodele amphibians. Developmental Biology, 396(1), 57–66. https://doi.org/https://doi.org/10.1016/j.ydbio.2014.09.021

Mescher, A. L. (1976). Effects on adult newt limb regeneration of partial and complete skin flaps over the amputation surface. Journal of Experimental Zoology, 195(1), 117–127. https://doi.org/https://doi.org/10.1002/jez.1401950111

Muneoka, K., Fox, W. F., & Bryant, S. V. (1986). Cellular contribution from dermis and cartilage to the regenerating limb blastema in axolotls. Developmental Biology, 116(1), 256–260. https://doi.org/https://doi.org/10.1016/0012-1606(86)90062-X

Nacu, E., Gromberg, E., Oliveira, C. R., Drechsel, D., & Tanaka, E. M. (2016). FGF8 and SHH substitute for anterior–posterior tissue interactions to induce limb regeneration. Nature, 533(7603), 407–410. https://doi.org/10.1038/nature17972

Niswander, L., Jeffrey, S., Martin, G. R., & Tickle, C. (1994). A positive feedback loop coordinates growth and patterning in the vertebrate limb. Nature, 371(6498), 609–612.

https://doi.org/10.1038/371609a0

Otsuki, L., & Tanaka, E. (2021). Positional Memory in Vertebrate Regeneration: A Century's Insights from the Salamander Limb. Cold Spring Harbor Perspectives in Biology, 14, a040899. https://doi.org/10.1101/cshperspect.a040899

Parr, B. A., & McMahon, A. P. (1995). Dorsalizing signal Wnt-7a required for normal polarity of D–V and A–P axes of mouse limb. Nature, 374(6520), 350–353. https://doi.org/10.1038/374350a0

Poulin, M. L., Patrie, K. M., Botelho, M. J., Tassava, R. A., & Chiu, I.-M. (1993). Heterogeneity in the expression of fibroblast growth factor receptors during limb regeneration in newts (Notophthalmus viridescens). Development, 119(2), 353–361. https://doi.org/10.1242/dev.119.2.353

Riddle, R. D., Ensini, M., Nelson, C., Tsuchida, T., Jessell, T. M., & Tabin, C. (1995). Induction of the LIM homeobox gene Lmx1 by WNT6a establishes dorsoventral pattern in the vertebrate limb. Cell, 83(4), 631–640. https://doi.org/https://doi.org/10.1016/0092-8674(95)90103-5

Riddle, R. D., Johnson, R. L., Laufer, E., & Tabin, C. (1993). Sonic hedgehog mediates the polarizing activity of the ZPA. Cell, 75(7), 1401–1416. https://doi.org/https://doi.org/10.1016/0092-8674(93)90626-2

Sader, F., & Roy, S. (2022). Tgf-β superfamily and limb regeneration: Tgf-β to start and Bmp to end. Developmental Dynamics, 251(6), 973–987. https://doi.org/https://doi.org/10.1002/dvdy.379

Satoh, A., Gardiner, D. M., Bryant, S. V, & Endo, T. (2007). Nerve-induced ectopic limb blastemas in the axolotl are equivalent to amputation-induced blastemas. Developmental Biology, 312(1), 231–244. https://doi.org/https://doi.org/10.1016/j.ydbio.2007.09.021

Satoh, A., Makanae, A., Nishimoto, Y., & Mitogawa, K. (2016). FGF and BMP derived from dorsal root ganglia regulate blastema induction in limb regeneration in Ambystoma mexicanum. Developmental Biology, 417(1), 114–125. https://doi.org/https://doi.org/10.1016/j.ydbio.2016.07.005

Schloissnig, S., Kawaguchi, A., Nowoshilow, S., Falcon, F., Otsuki, L., Tardivo, P., Timoshevskaya, N., Keinath, M. C., Smith, J. J., Voss, S. R., & Tanaka, E. M. (2021). The giant axolotl genome uncovers the evolution, scaling, and transcriptional control of complex gene loci. Proceedings of the National Academy of Sciences, 118(15), e2017176118. https://doi.org/10.1073/pnas.2017176118

SHIMOKAWA, T., YASUTAKA, S., KOMINAMI, R., & SHINOHARA, H. (2013). Lmx-1b and Wnt-7a expression in axolotl limb during development and regeneration. Okajimas Folia Anatomica Japonica, 89(4), 119–124. https://doi.org/10.2535/ofaj.89.119

Stocum, D. L. (1982). Determination of axial polarity in the urodele limb regeneration blastema. Development, 71(1), 193–214. https://doi.org/10.1242/dev.71.1.193

Thomas, P. D., Kejariwal, A., Campbell, M. J., Mi, H., Diemer, K., Guo, N., Ladunga, I., Ulitsky-

Lazareva, B., Muruganujan, A., Rabkin, S., Vandergriff, J. A., & Doremieux, O. (2003). PANTHER: a browsable database of gene products organized by biological function, using curated protein family and subfamily classification. Nucleic Acids Research, 31(1), 334–341. https://doi.org/10.1093/nar/gkg115

Thornton, C. S. (1962). Influence of head skin on limb regeneration in urodele amphibians. Journal of Experimental Zoology, 150(1), 5–15. https://doi.org/https://doi.org/10.1002/jez.1401500103

Todd, T. (1823). On the process of reproduction of the members of the aquatic salamander. Quart J Sci Lit Arts Lib, 16, 84–86.

Tsai, S. (2020). Inhibition of Wound Epidermis Formation via Full Skin Flap Surgery During Axolotl Limb Regeneration. JoVE, 160, e61522. https://doi.org/doi:10.3791/61522

Ugur, S. A., & Tolun, A. (2008). Homozygous WNT10b mutation and complex inheritance in Split-Hand/Foot Malformation. Human Molecular Genetics, 17(17), 2644–2653. https://doi.org/10.1093/hmg/ddn164

Vieira, W. A., Wells, K. M., Raymond, M. J., De Souza, L., Garcia, E., & McCusker, C. D. (2019). FGF, BMP, and RA signaling are sufficient for the induction of complete limb regeneration from non-regenerating wounds on Ambystoma mexicanum limbs. Developmental Biology, 451(2), 146–157. https://doi.org/https://doi.org/10.1016/j.ydbio.2019.04.008

Vogel, A., Rodriguez, C., Warnken, W., & Belmonte, J. C. I. (1995). Dorsal cell fate specified by chick Lmxl during vertebrate limb development. Nature, 378(6558), 716–720. https://doi.org/10.1038/378716a0

Witte, F., Dokas, J., Neuendorf, F., Mundlos, S., & Stricker, S. (2009). Comprehensive expression analysis of all Wnt genes and their major secreted antagonists during mouse limb development and cartilage differentiation. Gene Expression Patterns, 9(4), 215–223. https://doi.org/https://doi.org/10.1016/j.gep.2008.12.009

Yamamoto, S., Kashimoto, R., Furukawa, S., Ohashi, A., & Satoh, A. (2022). Lmx1b activation in axolotl limb regeneration. Developmental Dynamics, 251(9), 1509–1523. https://doi.org/https://doi.org/10.1002/dvdy.476

Yang, Y., & Niswander, L. (1995). Interaction between the signaling molecules WNT7a and SHH during vertebrate limb development: Dorsal signals regulate anteroposterior patterning. Cell, 80(6), 939–947. https://doi.org/https://doi.org/10.1016/0092-8674(95)90297-X

Yonei-Tamura, S., Endo, T., Yajima, H., Ohuchi, H., Ide, H., & Tamura, K. (1999). FGF7 and FGF10 Directly Induce the Apical Ectodermal Ridge in Chick Embryos. Developmental Biology, 211(1), 133–143. https://doi.org/https://doi.org/10.1006/dbio.1999.9290

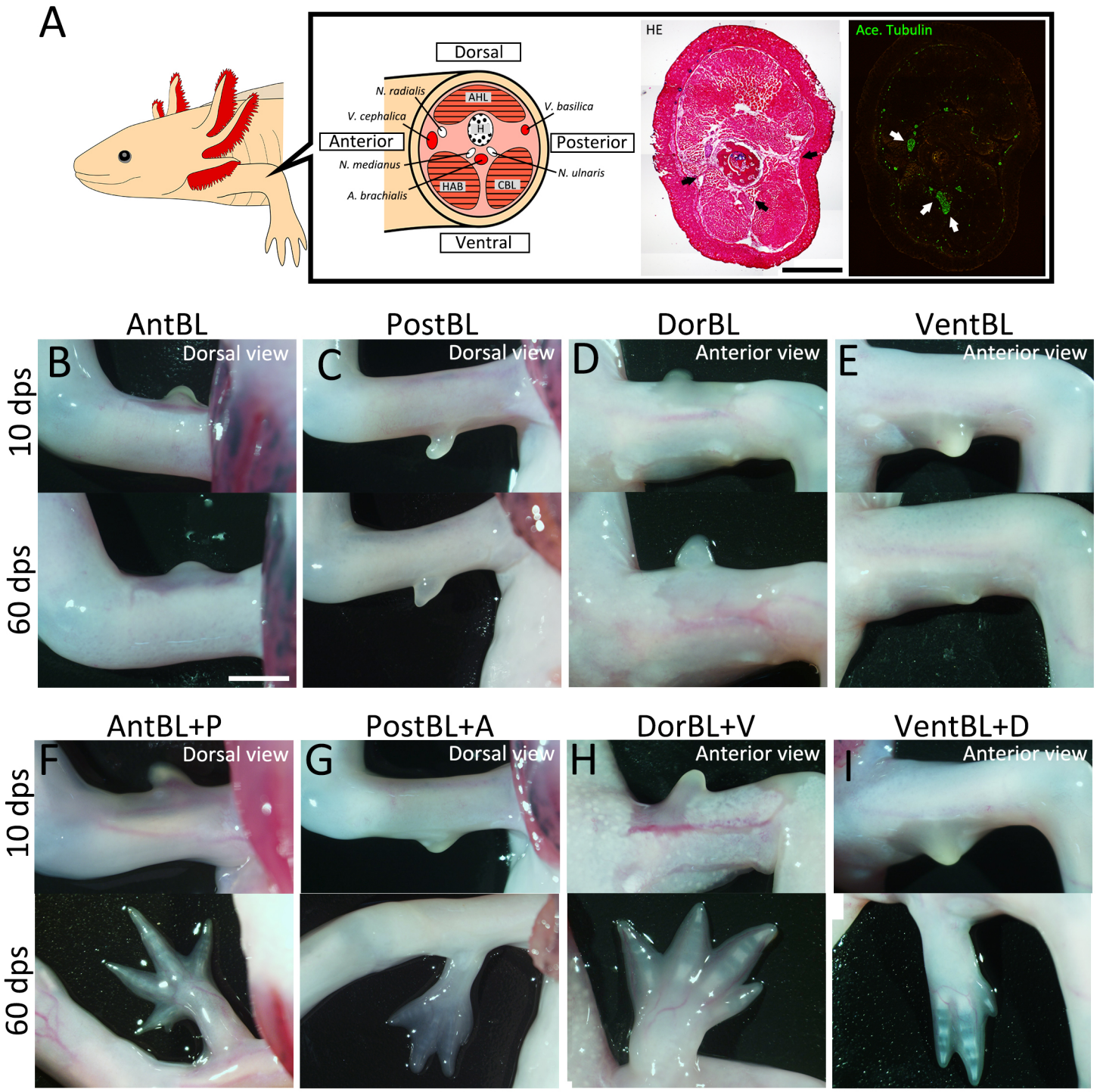

Yamamoto et al., 2025, Figure 1

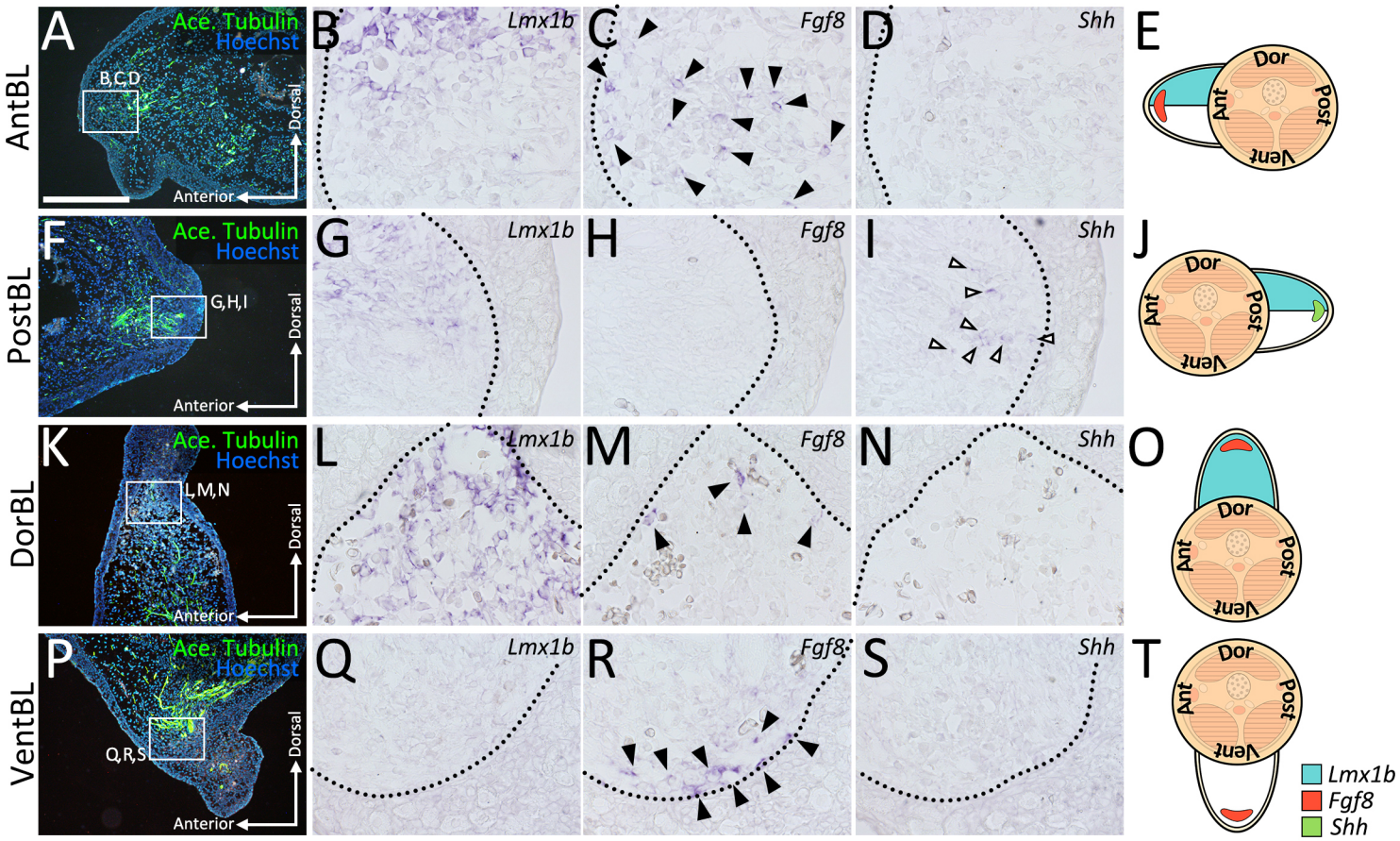

Yamamoto et al., 2025, Figure 2

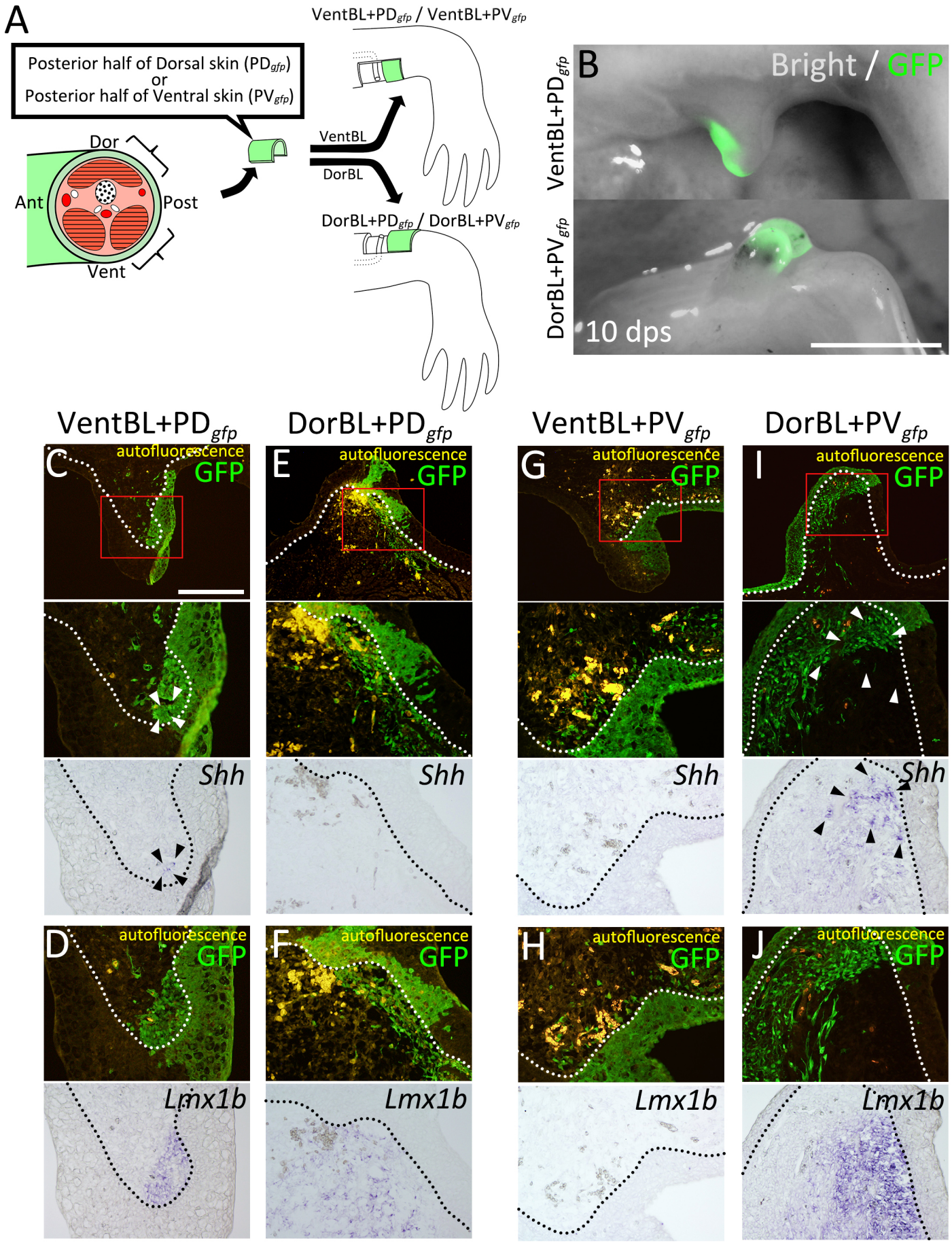

Yamamoto et al., 2025, Figure 3

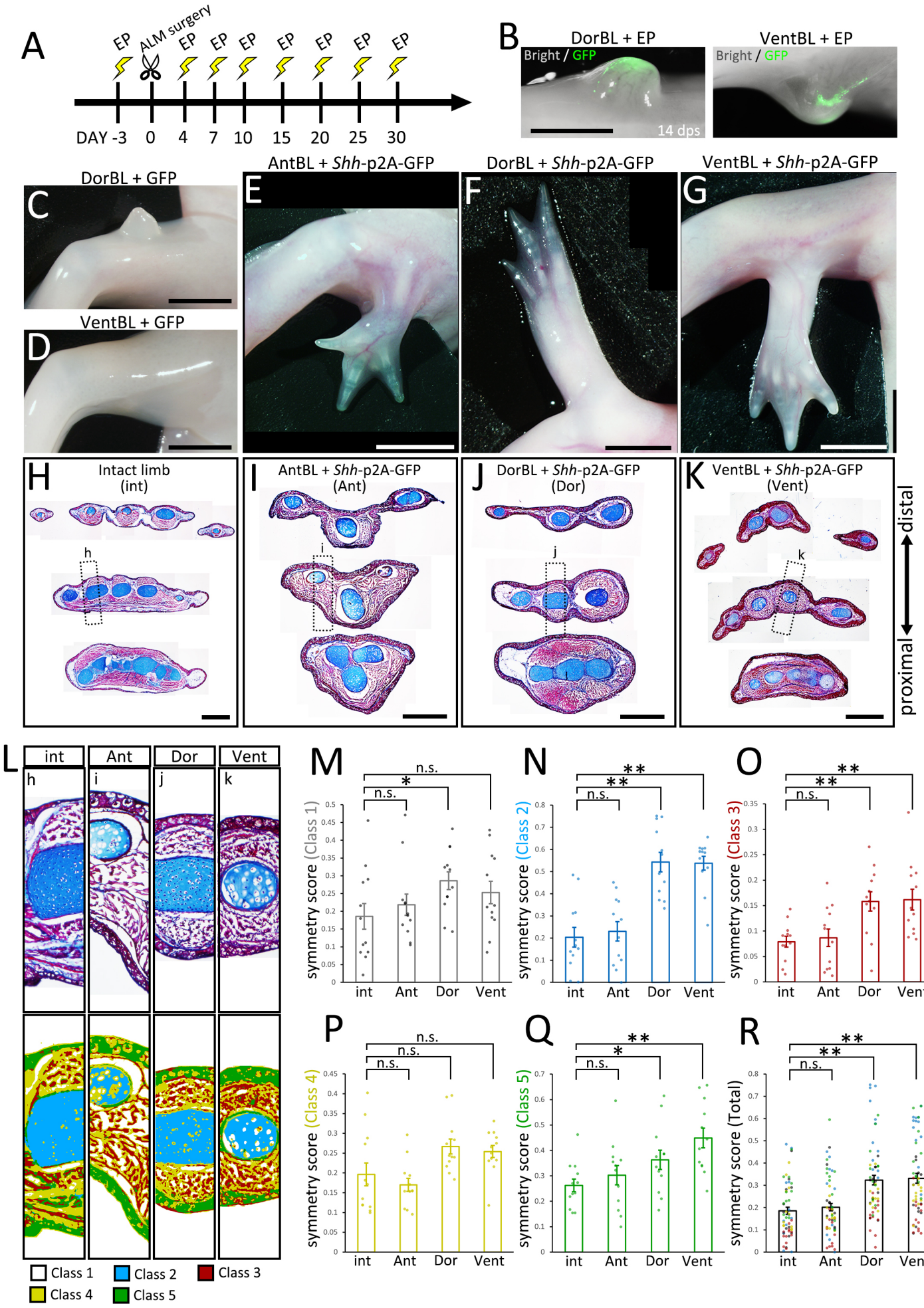

Yamamoto et al., 2025, Figure 4

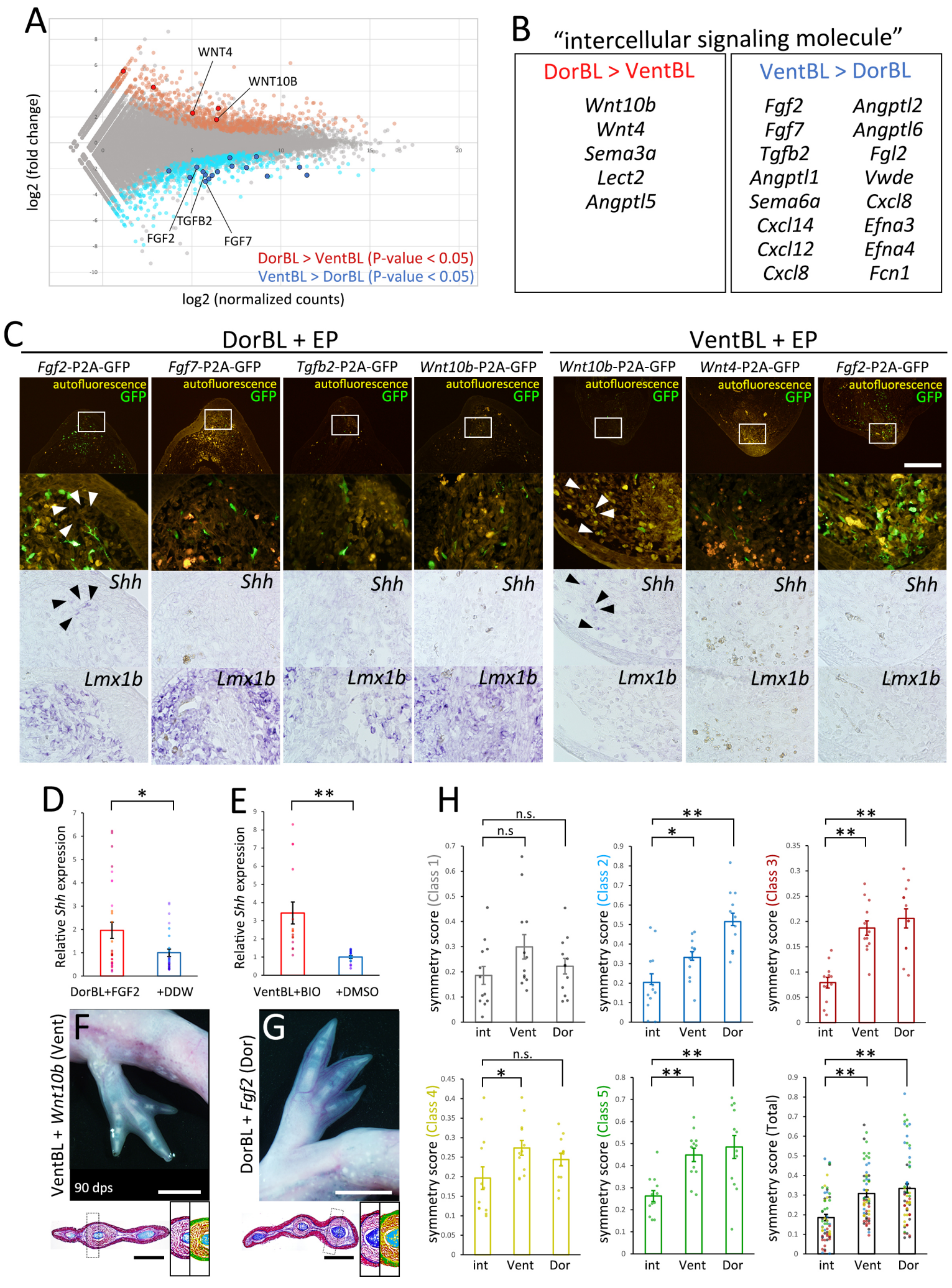

Yamamoto et al., 2025, Figure 5

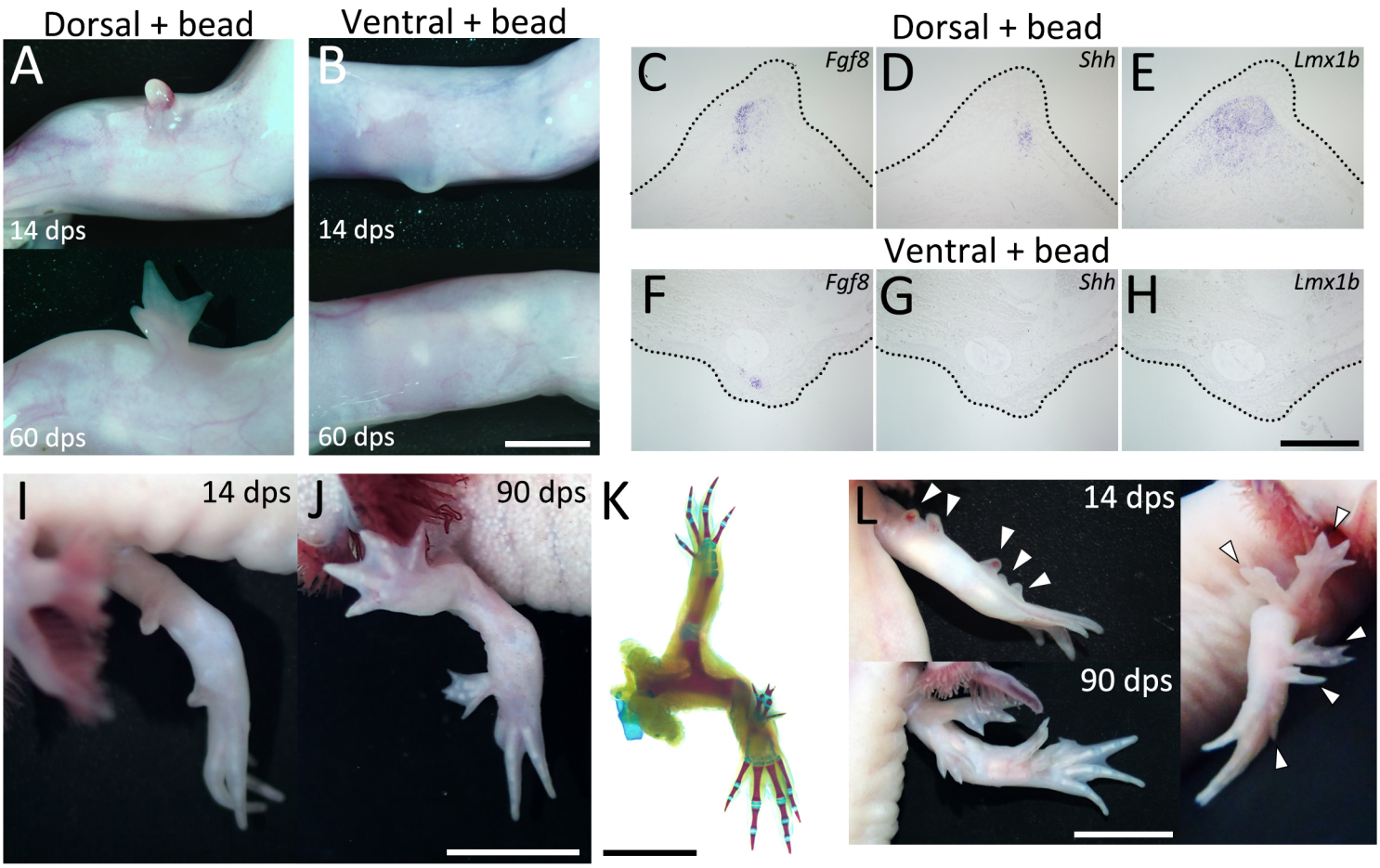

Yamamoto et al., 2025, Figure 6

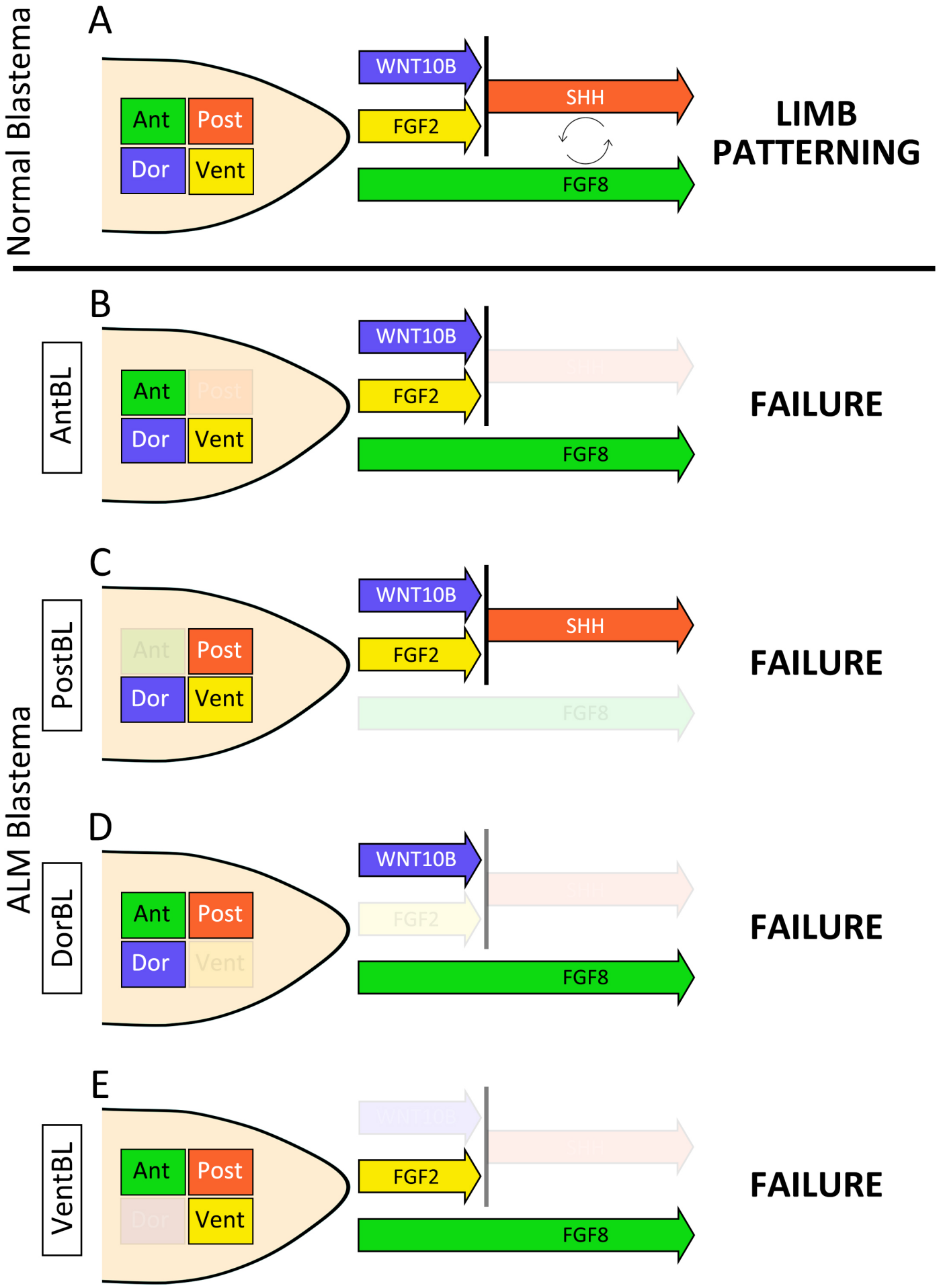

Yamamoto et al., 2025, Figure 7

	N	Regress		Bump		Limb	
AntBL	8	3	(37.5 %)	5	(62.5 %)	0	(0.0 %)
AntBL+P	9	0	(0.0 %)	1	(11.1 %)	8	(88.9 %)
PostBL	8	6	(75.0 %)	2	(25.0 %)	0	(0.0 %)
PostBL+A	7	2	(28.6 %)	1	(14.3 %)	4	(57.1 %)
DorBL	12	8	(66.7 %)	3	(25.0 %)	1	(8.3 %)
DorBL+V	14	5	(35.7 %)	2	(14.3 %)	7	(50.0 %)
VentBL	22	15	(68.2 %)	7	(31.8 %)	0	(0.0 %)
VentBL+D	11	2	(18.2 %)	2	(18.2 %)	7	(63.6 %)

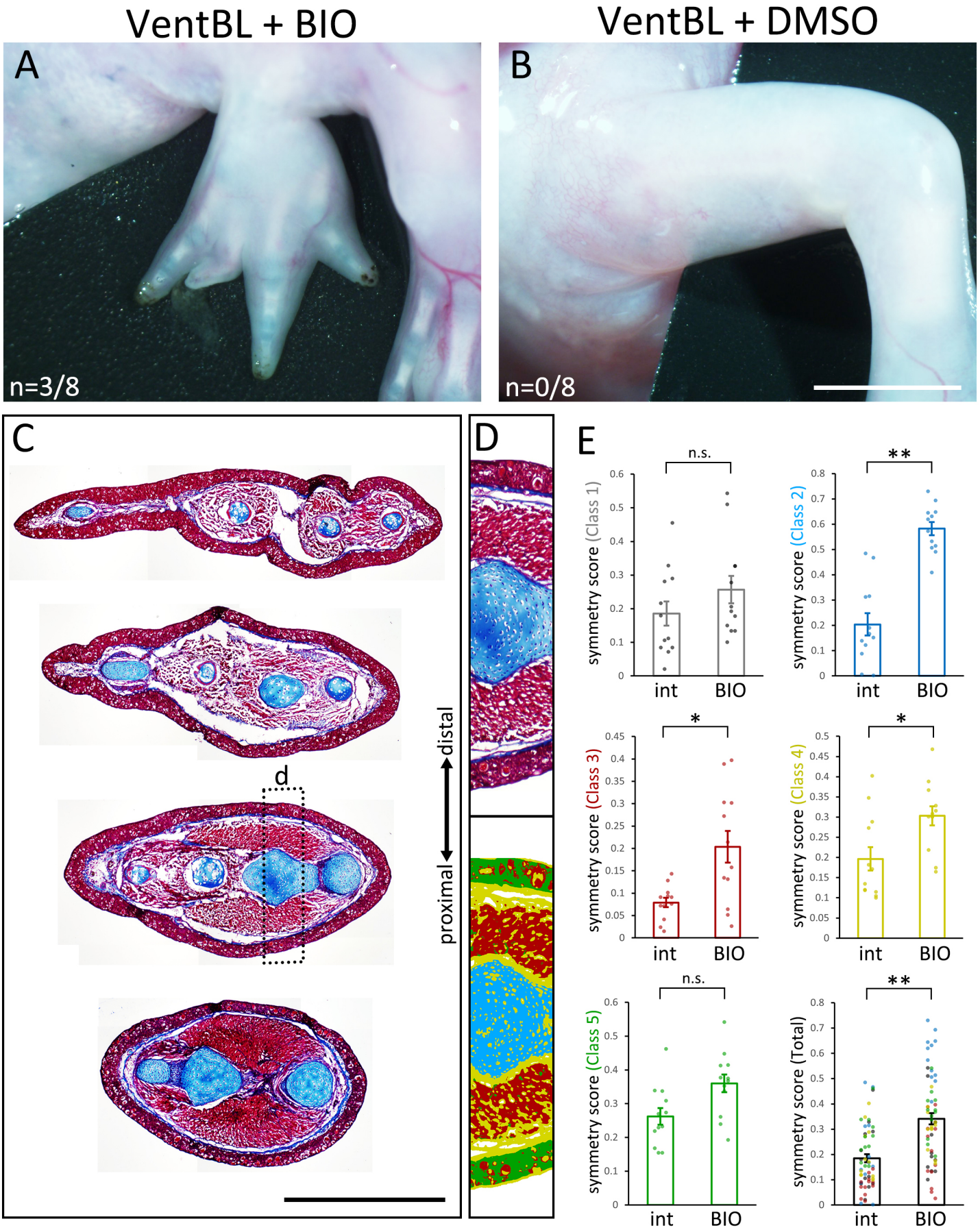

Yamamoto et al., 2025, Supplemental Figure 1